CHALMERS
UNIVERSITY OF TECHNOLOGY

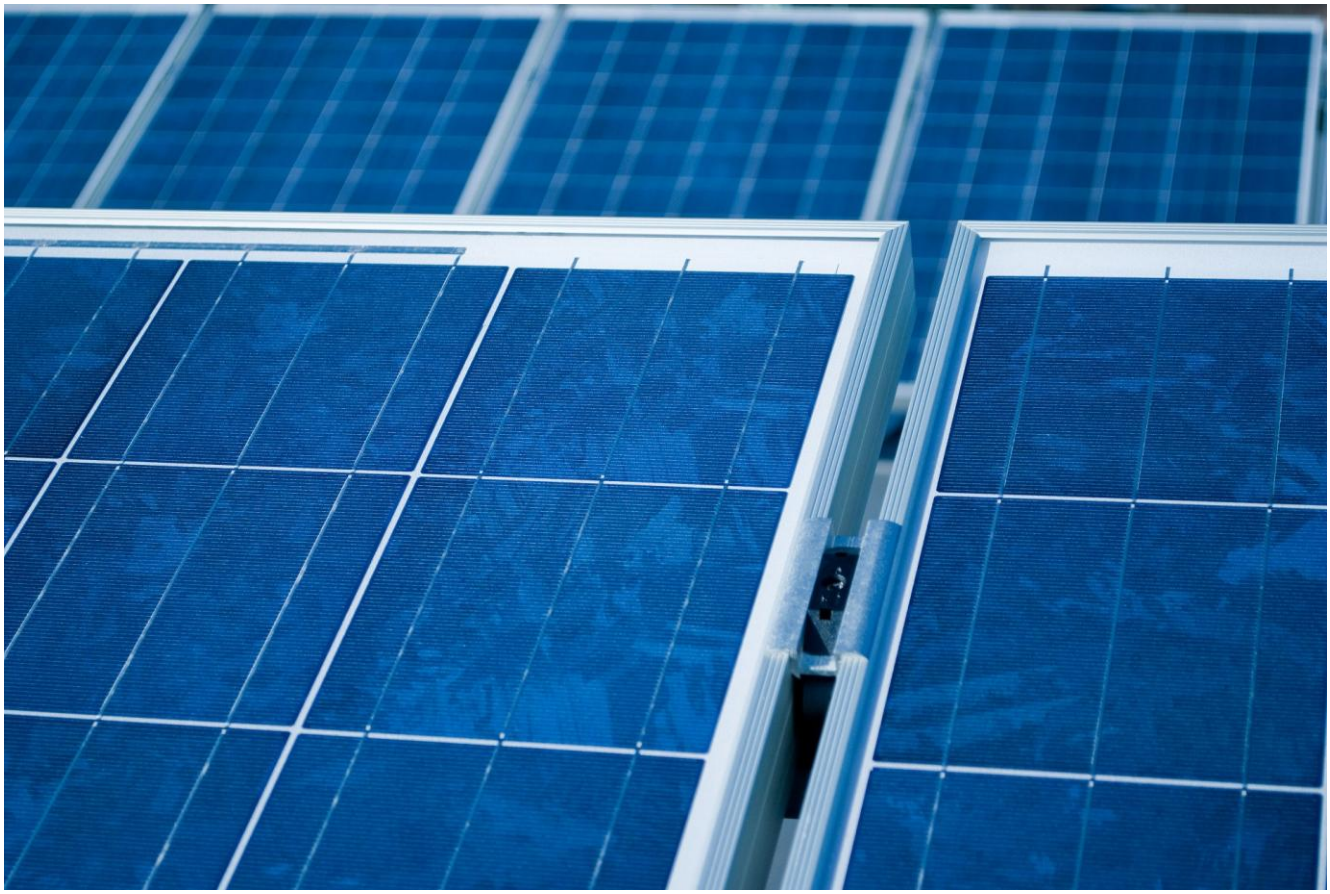

Modeling of Photovoltaic System with Power Smoothing for Integration in Power Systems

Master's thesis in Electric Power Engineering

MARCUS FRANZÉN ERIKSSON

Department of Energy and Environment
CHALMERS UNIVERSITY OF TECHNOLOGY
Gothenburg, Sweden 2015

Modeling of Photovoltaic System with Power Smoothing for Integration in Power Systems

MARCUS FRANZÉN ERIKSSON

Department of Energy and Environment
CHALMERS UNIVERSITY OF TECHNOLOGY
Gothenburg, Sweden 2015

Modeling of Photovoltaic System with Power Smoothing for Integration in Power Systems
MARCUS FRANZÉN ERIKSSON

Tutor: Mattias Persson
Examiner: Peiyuan Chen

Department of Energy and Environment
Chalmers University of Technology
SE-412 96 Göteborg
Sweden
Telephone + 46 (0)31-772 1000

Cover:
[PV panels on the roof of Älvstranden Utveckling's building LP3 at Lindholmen Science Park, Norra Älvstranden in Gothenburg. Photo by Per Hederstedt.]

[Chalmers reproservice]
Gothenburg, Sweden 2015

Modeling of Photovoltaic System with Power Smoothing for Integration in Power Systems
MARCUS FRANZÉN ERIKSSON
Department of Energy and Environment
Chalmers University of Technology

Abstract

Solar PV was the second largest installed power capacity in the EU 2014 and the rate at which PV is installed in Sweden has doubled each year for the last four years. Both the intermittent nature of PV power and the fact that PV systems do not provide any system inertia can cause a reduced frequency quality in the power system. Due to the fast growth of the PV market, it is of interest to develop methods which reduce PV systems' negative impacts on the power system frequency quality.

In this project, a power smoothing algorithm is developed and implemented in a modeled PV system. The PV system is connected to a simplified power system model in which the peak PV power constitute 10 % of the total power production and the remaining power is produced by a hydro power plant. An analysis of the frequency quality with and without smoothing has been conducted when logged irradiance data from the month of April 2015 is used as input to the PV system. The analysis shows that the smoothing algorithm improves the frequency quality in the simplified power system model. The mean- and maximum positive frequency deviations are improved (reduced) by approximately 40 % and 50 % respectively. Furthermore, the mean- and maximum Rate of Change of Frequency (ROCOF) are improved (reduced) by 20 %. The time during which the frequency goes above 50.9 Hz is reduced from 207 seconds to zero seconds. The time during which the frequency is above 50.5 Hz is reduced from 8.8 % to 0.4 % and the time during which the frequency goes below 49.5 Hz is reduced from 8.9 % to 5.5 %. The energy loss due to the use of the smoothing algorithm was 0.27 %. This can be compared to the average degradation of PV systems, which is around 0.5 % per year.

Furthermore, an existing method to characterize a PV panel using measurements is further developed in this project. The further developed method results in a PV panel model that, when compared to the measured PV panel characteristics, gives a residual sum of squares (RSS) of 1.3. Another method, which uses a European standard to find model parameters, has also been tested. However, the difference between the model and the measured PV panel characteristics is higher using this method, with the RSS of 3.17. Thus, the method further developed in this project gives a more accurate fit in terms of RSS error.

Keywords: Photovoltaic system modeling, power smoothing, ramp rate control, ramp limit, frequency control, frequency quality, PV panel modeling, PV system, smart grid, distributed generation.

Acknowledgements

The idea to do this project came from my tutor, Mattias Persson, who has contributed with very valuable feedback and support throughout the entire project – thank you very much for that! Thank you Magnus Ellsen for all the help with the logging equipment, for interesting discussions and for teaching me a lot of practical things. A special thanks to Ingmar Svensson at the Technical Research Institute of Sweden, SP, for taking the time to do measurements and provide me with PV panel data, it has been very valuable for the project. Thank you Peiyuan Chen for the feedback and interesting discussions. Thanks to Ken Ryrbo for being my opponent at the thesis presentation. I would also like to thank Johan Paradis at Paradisenergi for helping me to find logging equipment and for good advice during the project. Thank you Ingemar Mathiasson for helpful and interesting discussions. Thanks to Odyssefs Lykartsis for always having such useful advice, this time regarding simulation. Thank you Detlef Mencke at Ingenieurbüro Mencke & Tegtmeyer for very good support regarding the irradiance sensor and thank you Jonas Maki at National Instruments for very good support regarding the logging equipment.

Abbreviations

E	Irradiance [W/m^2]
I_D	Diode current [A]
I_L	Photon-generated current [A]
I_{MPP}	Current at the maximum power point [A]
IncCond	Incremental conductance
I_{out}	Output current [A]
I_{Rp}	Current through the resistance R_p [A]
$Irr_{deriv,max}$	Steepest derivative found in the logged irradiance data [W/s]
$Irr_{max,30}$	Maximum irradiance difference within 30 second found in the irradiance data [W]
I_{sc}	Short circuit current [A]
IV-curve	Current and voltage curve
I_0	Reverse bias saturation current [A]
k	Power ramp rate [W/s]
k_b	The Boltzmann constant [J/K]
MPP	Maximum power point
MPPT	Maximum power point tracker
N	Number of previous power values consider in the smoothing algorithm
n	Diode ideality factor
N_c	Number of series connected photovoltaic cells
P_{MPP}	Power at the maximum power point [W]
P_n	Power n iterations before the present iteration in the smoothing algorithm [W]
P_{now}	Power at the present iteration in the smoothing algorithm [W]
p.u.	Per unit
PV	Photovoltaic
PV-curve	Power and voltage curve
q	Elementary charge of an electron [C]
ΔP_{tot}	Sum of power differences in the smoothing algorithm
ΔP_{trigg}	Sum of power differences at linear power distribution in the smoothing algorithm
ROCOF	Rate of change of frequency [Hz/s]
R_p	Parallel resistance [Ω]
R_s	Series resistance [Ω]
RSS	Residual sum of squares
STC	Standard test conditions
T	Photovoltaic cell temperature [K]
V_D	Diode voltage [V]
$V_{D_{MPP}}$	Diode voltage at the maximum power point [V]
V_{MPP}	Voltage at the maximum power point [V]
V_{oc}	Open circuit voltage [V]
V_{out}	Output voltage [V]
V_{ref}	Voltage reference [V]
$V_{Rs_{MPP}}$	Voltage over R_s at the maximum power point [V]
V_t	Thermal voltage [V]

Contents

1 Introduction

1.1 Background and motivation

Since 2006 the Nordic power system has experienced a clear trend towards lower frequency quality [1]. The frequency quality may be worse if there is an increase in the amount of renewable intermittent power sources in the power system, like wind and solar [2]. Solar photovoltaic (solar PV) power was the second largest installed power capacity in the EU 2014 and the rate at which PV is installed in Sweden has doubled each year for the last four years [3], [4]. Both the intermittent nature of PV power and the fact that PV systems provide no inertia may cause a reduced frequency quality in the power system [5]. Due to the fast growth of the PV market, it is of interest to develop methods which reduce PV systems' negative impacts on the power system frequency quality.

The focus of this project is on the development and validation of a method that smoothes the output power from a PV system by limiting the rate of change of its output power. When smoothing the output power, frequency quality improvements can be expected in certain power system configurations. One such configuration could, for example, be the Swedish power system during the summer months in a few years when the peak power is relatively low compared to the wintertime and the installed PV capacity has increased. PV capacity might then constitute a considerable part of the total power capacity in the system and power smoothing might therefore contribute to a more stable power system frequency. Likewise, power smoothing might be useful in countries like Puerto Rico, South Africa and Mexico, where new grid codes limit the allowed ramp rate for PV power output. In Puerto Rico, the limit is set to 10 % of the PV systems' peak-power/minute and in Mexico the limit is set to between 1-5 % of the peak-power/minute [6]. Furthermore, in India there are plans to build a 4 GW PV system [7]. Such a system might at times correspond to a relatively high percentage of the total power production in the power system. Limiting the power ramp rate from such a PV system properly would improve the frequency quality. Moreover, power smoothing could be useful during a solar eclipse, like the one that occurred in Europe recently [8]. A solar eclipse can cause significant frequency disturbances if a high percentage of the power to the grid is provided by PV systems. Being able to ramp the power might improve frequency stability significantly. In Italy, many PV systems were disconnected during the recent solar eclipse. A possibility to limit the power ramp rate could have resulted in significant economic savings for these PV systems' owners during this solar eclipse, as the need to disconnect systems might have been reduced. In addition, a limited power ramp rate for PV systems might help during a black start of a power system.

1.2 Aim

The aim of the project is to develop and evaluate an algorithm that smoothes the output power from a PV system when clouds pass by, so as to improve the frequency quality in the power system. Another aim is to characterize a PV panel and use the panel parameters as base for a PV system model in which the smoothing algorithm is implemented.

1.3 Tasks

The following tasks are to be carried out:

- Arrange an irradiance logging setup and log irradiance during one month at Chalmers research facility on the island of Hönö.

- Model a simplified PV system. The input should be irradiance (W/m^2) and the output should be DC power (W). The model should include a PV panel and a maximum power point tracker (MPPT). The PV panel should be of polycrystalline type as it is the dominant technology on the PV market [9].

- Develop and evaluate an algorithm that smoothes the output power from a PV system. Compare the algorithm with the conventional use of a MPPT in terms of energy loss. Input data to the PV system should be the irradiance data logged on the island of Hönö.

- Use a model for frequency regulation by a typical hydro power plant and combine it with the PV system model. This is to create a representation of a simplified power system. Compare the power smoothing algorithm and conventional use of MPPT in terms of frequency quality.

1.4 Delimitations

These simplifications are made in the PV system model:

- The PV panel part of the model is based on a model for a PV cell.

- The PV system is based on the characteristics of a polycrystalline PV panel.

- The PV system consists of a PV panel model and a variable voltage source (representing a DC-DC converter input). The voltage reference to the variable voltage source is given by the MPPT/smoothing algorithm.

- The effects of partial shading on the PV system is not modeled. The irradiance is considered homogenous over the whole PV system.

2 Related photovoltaic theory

2.1 Grid connected photovoltaic systems

A grid connected PV system converts the sun's irradiance into electric power and transfer this power to the grid. The system consists of several components. A generic overview of a grid connected PV system is presented in Figure 1.

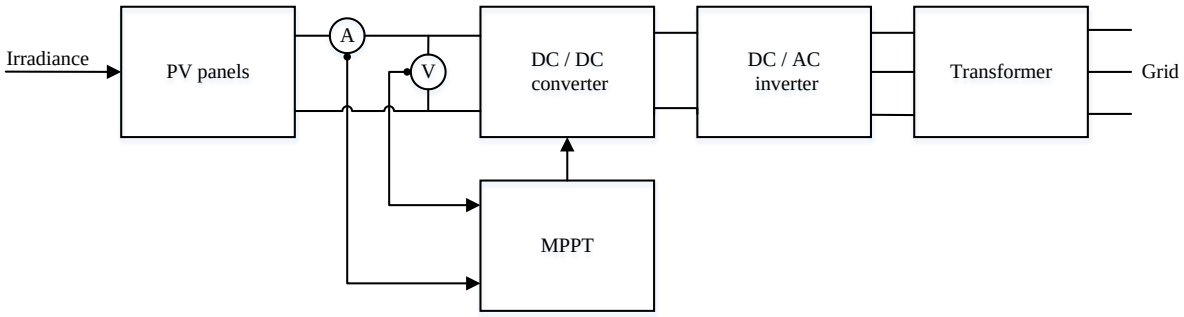

Figure 1: Generic overview of a grid connected PV system.

The PV panels generate DC voltage and DC current. The voltage over the panels is controlled by a DC/DC converter, which receives a reference voltage from a MPPT. The MPPT outputs the voltage reference based on measured voltage and current on the DC-link between the panels and the DC/DC converter. The inverter inverts the DC voltage and current into AC, which is then fed to the grid. A PV system has certain current-voltage characteristic, or IV characteristic, which is a scaled version of the IV characteristic for each PV panel used in the system. These characteristics can be illustrated by an IV-curve, see Figure 8.

2.2 Maximum power point tracker theory

A MPPT control the voltage on the DC side of a PV system, i.e. the DC-link between the PV panels and the DC/DC converter, by giving a reference voltage (usually converted into a duty cycle reference) to the DC/DC converter. The purpose of the MPPT is to maximize the power transfer on the DC link [10]. The point on the IV-curve that gives the maximum power, i.e. the maximum power point (MPP), can be found by multiplying the voltage and the corresponding current for all voltages and currents on the curve. In Figure 8, the MPP is indicated on an IV-curve and it can be observed that it is located at the same voltage level as the maximum point on the power-voltage curve (PV-curve).

Maximum power point tracking can be performed using many different methods. In [10] a survey of over 90 papers on MPPT techniques is presented. Many of these papers focus on Hill Climbing and Perturb and Observe (P&O) techniques, which are two methods to realize the same result; perturbation of the voltage and observation of the change in power. In these methods, the voltage and current is measured and multiplied after each voltage perturbation in order to find whether the change lead to an increase or a decrease in power. For example, if the voltage is increased and the power is also increased, the next change in voltage will be an increment. If, on the other hand, the power is decreased, the next change in voltage will be a decrement. In this way, the MPPT can

make the systems operating point oscillate very close to the MPP. The voltage step-size of the MPPT decides the magnitude of the oscillation as well as the speed at which the operating point approach the MPP. The speed is also dependent on how often the voltage changes.

Another method, which is very similar to those previously described, is the Incremental Conductance (IncCond). To track the MPP, it uses the fact that the derivative of the PV-curve is zero at the MPP (see Figure 8). A more elaborating explanation of the IncCond method is found in section 5.1. A much simpler, but yet functional MPPT technique is the Fractional Open-Circuit Voltage. It uses the fact that there is a close to linear relation between V_{oc} and V_{MPP}. By scaling V_{oc} with a factor k_f, V_{MPP} can be approximated. This technique is very easy and cheap to implement, but does not result in true MPP tracking and cannot handle partial shading well. There are also far more complex MPP tracking techniques, for example Fuzzy Logic Control and control by Neural Networks. The Fuzzy logic control converts input signals, for example the power and the derivative of the power, into linguistic variables which are compared to a lookup table. Depending on the codification of the lookup table, output signals are generated, for example a preferred voltage reference change. The Neural network control is similar to Fuzzy logic in the sense that certain rules control how the input signals should be interpreted. Though, these rules change over time as the neural network is trained and an improved control strategy is therefore achieved over time.

3 Solar irradiance logging

In this project a setup was designed and built to measure and log solar irradiance at Chalmers research facility on the island of Hönö, near Gothenburg. The logged irradiance is used as input to the constructed PV model to evaluate its behavior in realistic operating conditions. By logging irradiance during a longer period of time, test signals that reflect typical irradiance variations were identified and constructed. These test signals are used as input to the PV model to analyze the performance of MPPT and smoothing algorithms.

3.1 Logging equipment requirements

A crystalline silicon solar panel is used as a basis for the PV model in this project, as it is the most common PV technology [9]. It is therefore suitable to use a crystalline silicon based irradiance sensor when logging the irradiance in order to mimic the behavior of the solar panel regarding thermal behavior and spectral absorption. Other features required from the irradiance sensor are fast response time and robust design for outdoor use. The measured irradiance should also be temperature compensated to ensure that irradiance is logged correctly. These features are fulfilled by a sensor from Ingenieurbüro Mencke & Tegtmeyer GmbH, the SiS-13TC-T (see Appendix I), which was used for irradiance measurements. This sensor has a voltage output in the range of 0-10 V, thus the logging equipment has to be able to log a voltage signal within this range. Moreover, the signal needs to be sampled fast enough to capture rapid irradiance changes. These criteria are fulfilled by a logging device from National Instruments, NI-USB-6009, which was used for logging, see Appendix I.

3.2 Logging equipment setup

The NI-USB-6009 is connected to a computer and controlled from the software LabView [11]. To convert the voltage signal into irradiance it is multiplied by a factor of 130, see Appendix I. The complete logging setup was tested to verify that irradiance was logged accurately.

The test showed that even during no light, the NI-USB-6009 measured a voltage signal of 0.484 V, corresponding to an irradiance equivalent to approximately 65 W/m^2. Though, when measuring at the irradiance sensor output (without the NI-USB-6009 connected) with oscilloscope the output signal was found to be 0 V. A hypothesis of why this occurs is that the logger add this voltage due to its circuit structure and because the output impedance is high on the irradiance sensor. However, voltages above 0.484 V were logged accurately. In order to log voltages below 0.484 V, an operational amplifier, AD620AN from Analog Devices (see Appendix I), is connected as a voltage follower between the output of the sensor and input of the logging device. The voltage follower is coupled with both positive and negative voltage from a DC power supply (PULS ML30.106). The negative voltage supply allowed for the output of the voltage follower to be zero when the input voltage was zero, i.e. when the sensor is not irradiated.

To make the logging setup robust enough to log irradiance continuously over time, the logging equipment was installed in a metallic enclosure, see Appendix II. A schematic of the complete logging setup is presented in Figure 2.

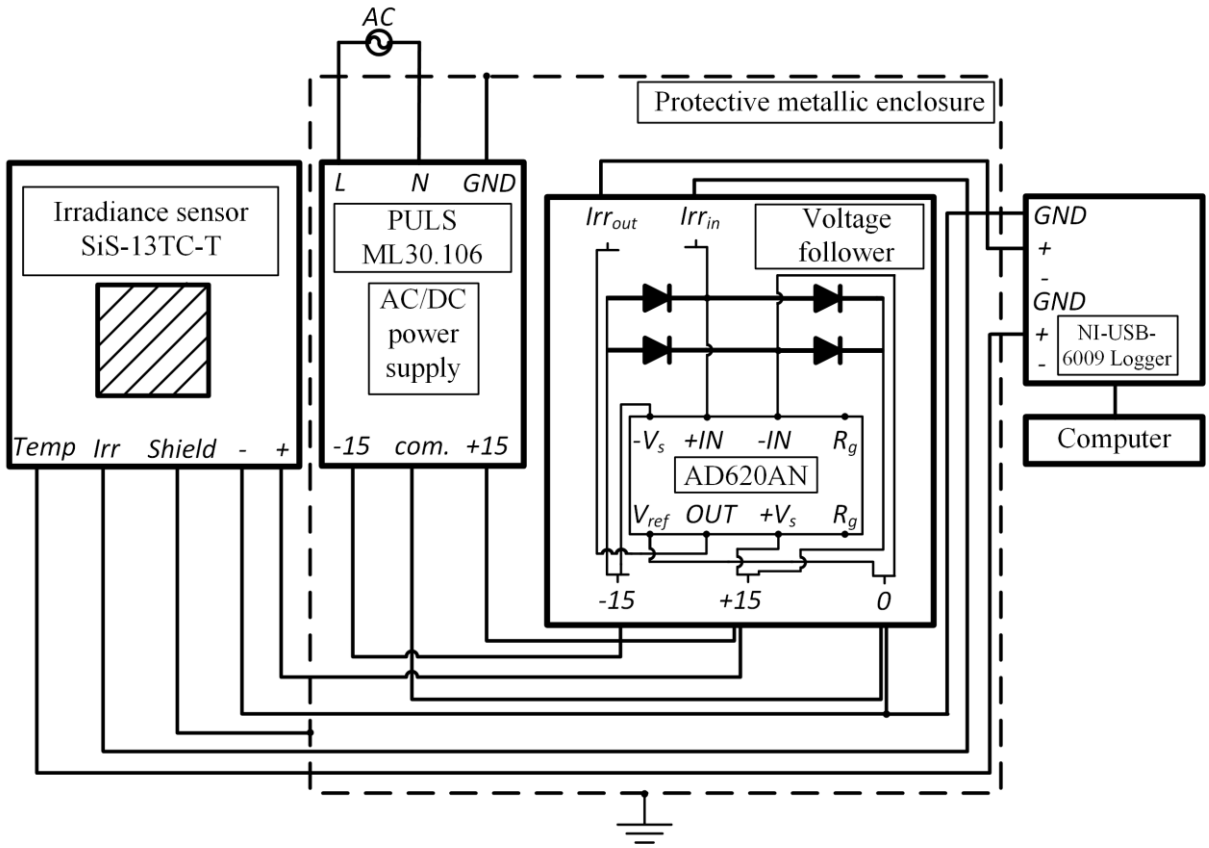

Figure 2: Logging setup including irradiance- and temperature sensor, DC power supply, voltage follower with protective diodes, logging device and computer. The DC power supply and voltage follower were encapsulated in a metallic box for protection and more convenient handling.

The logging setup includes irradiance sensor, DC power supply, voltage follower, NI-USB-6009 logging device and a computer. As the sensor was mounted outdoors, diodes were installed between the irradiance sensor output and the voltage follower input to protect from induced over voltages, e.g. caused by nearby lightning strikes. Datasheets for the irradiance sensor, voltage follower and logger is found in Appendix I.

3.3 Conclusions regarding logging setup

Tests were performed to verify the logging setup functionality. An elaborating description of these tests is presented in Appendix IV. From the tests it is concluded that a logging arrangement using SiS-13TC-T irradiation sensor, AD620AN connected as a voltage follower and NI-USB-6009 logging device can be used for the purpose of studying the characteristics and rate of change of irradiance above 85 W/m^2. A positive irradiance change within 300 ms and a negative irradiance change within 200 ms cannot be fully detected because of limitations in the sensor, but it is expected that this will not have any significant impact on further analysis in this project. The logging setup can be used to log irradiance below 85 W/m^2, but then a relatively long negative response time can be expected from the sensor. The irradiance was logged with 100 S/s (corresponding to 10 ms between each sample) in this project. A measurement noise of 2-4 W was measured between samples, thus no irradiance change within 10 ms with a magnitude below 4 W can be detected. However, no such fast and small changes in irradiance are considered relevant for

PV- and power system modeling. It can therefore be concluded that the chosen sample rate of 100 S/s is fast enough for irradiance logging in this project.

3.4 Logging data for use in modeling

To model the effects of power smoothing in a realistic way (see chapter 7), irradiance data for a longer period of time is needed. Therefore, the logging equipment was installed at Chalmers research facility on the island of Hönö near Gothenburg and irradiance was logged during April 2015 (a picture of the logging setup is found in Appendix II). The sensor is installed at an angle of 45° and an azimuth of 185°. Based on the logged irradiance, four different test signals were constructed for use in MPPT and power smoothing algorithm testing. The test signals types are step change, ramp, triangular and sinusoidal. More on why these specific signals are selected can be found in chapter 5 and 6. When analyzing the logged irradiance, it is found that the maximum irradiance difference within 30 seconds, 982 W/m^2, occurs on 27 of April. This difference is used as amplitude for all test signals and is denoted $Irr_{max,30}$. The reason for choosing this amplitude for the test signals is that it takes 30 seconds for the *frequency controlled disturbance reserve* in the Nordic power system to be fully activated [12]. A more elaborating explanation of why it is important to consider the frequency controlled disturbance reserve when choosing the amplitude for the test signals is presented in Chapter 7. The irradiance during 27 of April is shown in Figure 3, and the 30 seconds interval containing the maximum irradiance difference is indicated with two rings.

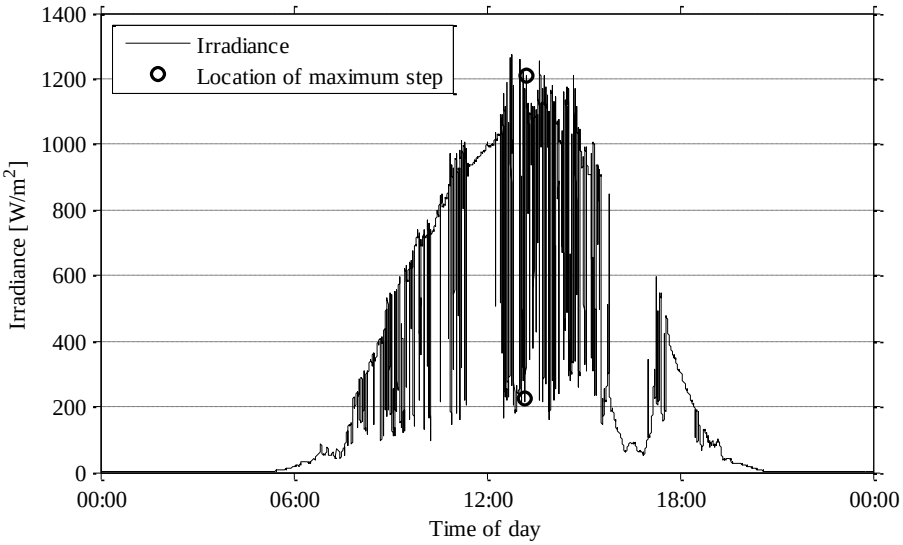

Figure 3: Irradiance on 27 April, where the maximum difference in irradiance within 30 seconds is found, 982 W/m^2.

To construct relevant ramp, triangular and sinusoidal test signals, the maximum derivative found in the logged irradiance is of interest. Though, the irradiance contains a measurement noise of approximately 2-4 W/m^2 peak-to-peak. This noise cause a high derivative between samples, and makes it difficult to separate a high derivative in the actual signal from one caused by noise. For this reason the irradiance signal is filtered. This is done using the LOWESS algorithm in MATLAB, which is an acknowledged method to smooth scattered data by local weighted linear regression [13], [14]. The principle is that a weighted linear regression is computed for a specified

number of samples around each sample in the data sequence. The specified number used when filtering the irradiance was set to 40, as it gave a smooth data sequence without losing any significant data. Specifically data at local sharp maxima and minima might be lost or recomposed with error when filtering is used. A comparison of the measured and filtered irradiance is seen in Figure 4. The irradiance data in Figure 4 were obtained during a test logging session on Chalmers campus in Johanneberg, Gothenburg on 3 of October 2014.

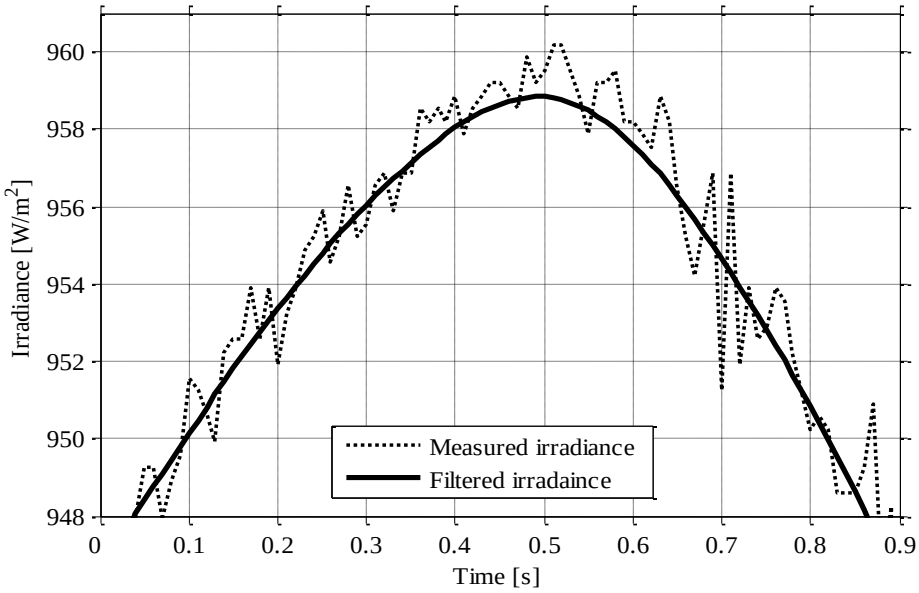

Figure 4: Measured and filtered irradiance during approximately one second on 3 of October 2014. The figure shows a local irradiance maximum.

From Figure 4 it can be concluded that the filtered irradiance signal follows the measured signal befittingly even at sharp maxima.

After filtering the signal, the derivative of the irradiance is evaluated. This is done by calculating the irradiance change between each sample. As the sampling rate is 100 S/s, each calculated irradiance change is multiplied by a factor of 100 to get the equivalent irradiance change per second. The steepest irradiance derivatives for each day in April are presented in Figure 5.

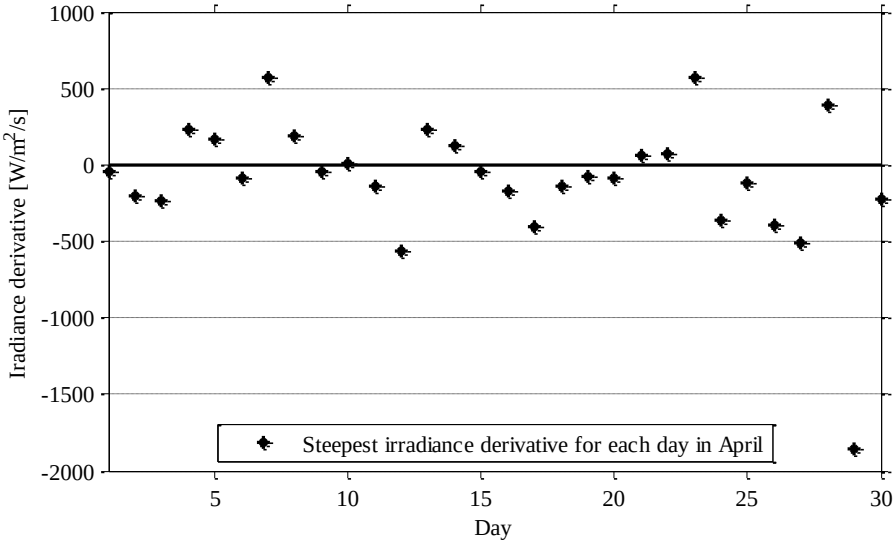

Figure 5: The steepest irradiance derivative for each day in April 2015.

In Figure 5 it can be seen that the steepest irradiance derivative, -1856 W/m^2/s, is found on 29 of April. Because of the large deviation from the steepest derivatives the other days of the month, and because of the characteristics of the irradiance change (see a short elaboration on this in Appendix IV), the steep derivative on April 29 has been considered an error in the data. Furthermore, as seen in Figure 5, the second steepest derivative occurs on April 7. It is 573 W/m^2/s and is denoted $Irr_{deriv,max}$. The $Irr_{deriv,max}$ is considered the steepest correctly measured derivative and has been used when constructing test signals in this project, see Section 5.2. The irradiance at the time when the maximum derivative occurs on April 7 is seen in Figure 6.

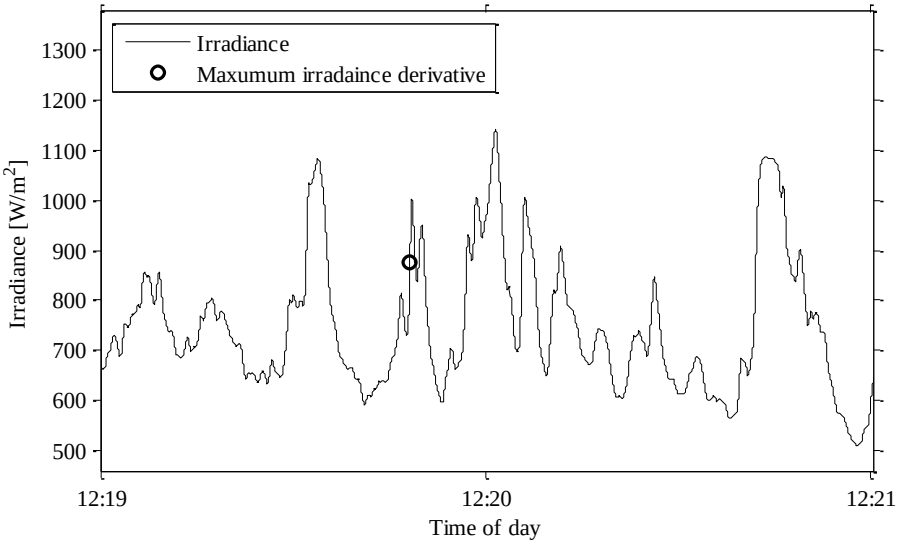

Figure 6: Irradiance at the time when the maximum irradiance derivative, 573 W/m^2/s, accurse on April 7.

From Figure 6 it can be concluded that there is a fast positive irradiance increase at the time when the maximum derivative occurs. This indicates that the maximum derivative is caused by an actual irradiance increase and not by noise.

4 Modeling of photovoltaic panel

In this project a PV system is modeled to evaluate the effects of smoothing PV output power. The behavior of a PV system depends on the characteristics of the PV panels in the system. Therefore it is important to find a realistic model for a PV panel.

4.1 Equivalent model for a photovoltaic cell

A PV panel can be modeled by initially using an equivalent circuit for a PV cell, see Figure 7.

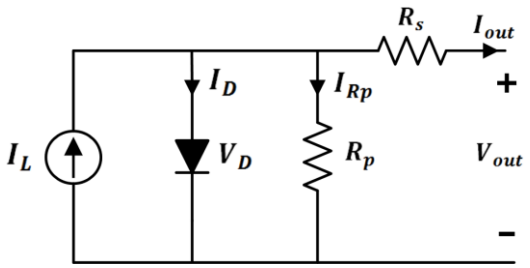

Figure 7: Equivalent circuit for a PV cell.

The circuit in Figure 7 is often referred to as the *one diode model* of a PV cell [15], [16]. The one diode model is considered by many to offer a good balance between simplicity and accuracy [15]. The parameters introduced in Figure 7 are summarized in Table 1.

Table 1: Summary and brief explanations of parameters found in Figure 7.

$\boldsymbol{I_L}$	Photon-generated current [A]
$\boldsymbol{I_D}$	Diode current [A]
$\boldsymbol{V_D}$	Diode voltage [V]
$\boldsymbol{R_s}$	Series resistance [Ω]
$\boldsymbol{R_p}$	Parallel resistance [Ω]
$\boldsymbol{I_{Rp}}$	Current through R_p [A]
$\boldsymbol{I_{out}}$	Output current [A]
$\boldsymbol{V_{out}}$	Output voltage [V]

The photon-generated current I_L is proportional to the irradiance towards the PV cell according to

$$I_L = I_{L0} \cdot \frac{E_r}{E_{r0}} \tag{1}$$

where I_{L0} is the photon-generated current for a specific irradiance E_{r0} and E_r is the irradiance onto the cell [17]. The diode current, I_D, can be described by the Shockley diode equation

$$I_D = I_0(e^{\frac{V_D}{N_c n V_t}} - 1) \tag{2}$$

where I_0 is the reverse bias saturation current, V_D is the voltage across the diode, n is the diode ideality factor and N_c is the number of series connected cells [18]. Typically, $1 < n < 2$ [19]. V_t is a thermal voltage which can be expressed as

$$V_t = \frac{k_b T}{q} \tag{3}$$

where k_b is the Boltzmann constant, T is the cell temperature and q is the magnitude of charge of an electron, i.e. the elementary charge. V_t at 25 °C is 25.69 mV [19].

The parameters R_s and R_p represent losses in the PV cell. To give a more elaborate explanation of these parameters, a short description of the cell structure is required. A silicon PV cell consists of two semiconducting layers, one n-doped (emitter) layer and one p-doped (collector) layer. The boundary between these two layers forms a pn-junction. On top of the emitter layer there are thin bands of conductors arranged in a grid structure to conduct the photon generated current. The parameter R_s represents resistive losses due to resistivity in the semiconductor, 2D conduction mechanisms in the emitter layer and resistivity in the conductors and contacts. The parameter R_p represents shunt resistance which takes into account all parallel losses across the semiconductor junction due to partial junction short circuits [20].

A PV panel consists of many series connected PV cells. When connecting several cells in series, the current through them will not increase, but the voltage between the first and last series connected cell will increase with each added cell. This makes the output voltage of a PV panel proportional to the number of cells in the panel. In further modeling, R_s will represent the equivalent series resistance of all the cells in the PV panel and R_p will represent the equivalent parallel resistance of all the cells in the PV panel. A large R_p and a small R_s indicate a solar panel with low internal losses.

The current and voltage characteristics of a PV panel can be illustrated by an IV-curve. By multiplying voltage and current at each operating point, a PV-curve can be constructed from the IV characteristics. An IV-curve with corresponding PV-curve for a PV panel, Windon Tatu 255 Multi, is illustrated in Figure 8. This PV panel is used in further modeling in this project, see Section 4.4

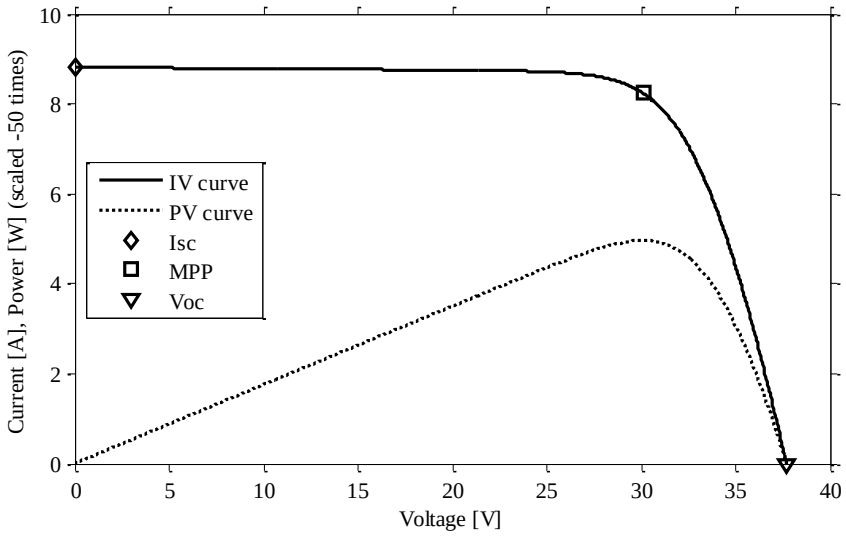

Figure 8: Modeled IV- and PV-curves for the PV panel Windon Tatu 255 Multi. Significant operating points are indicated on the IV-curve.

In Figure 8, three operating points are indicated on the IV-curve. The leftmost is operation at short circuit, which gives I_{sc} (marked by ◊). The second is operation at the maximum power point, MPP, which gives I_{MPP} and V_{MPP} (marked by □). The third is operation at open circuit, giving V_{oc} (marked by ∇). These points provide important information regarding the performance of the PV panel and are often included in PV panel datasheets. Henceforth, these points will be referred to as the *significant operating points*.

The characteristics of an IV-curve are greatly dependent on R_s and R_p. The rightmost part of an IV-curve is strongly affected by R_s while the leftmost part is mainly affected by R_p. These effects are illustrated in Figure 9. Further explanations regarding modeling procedures are presented in Section 4.4.

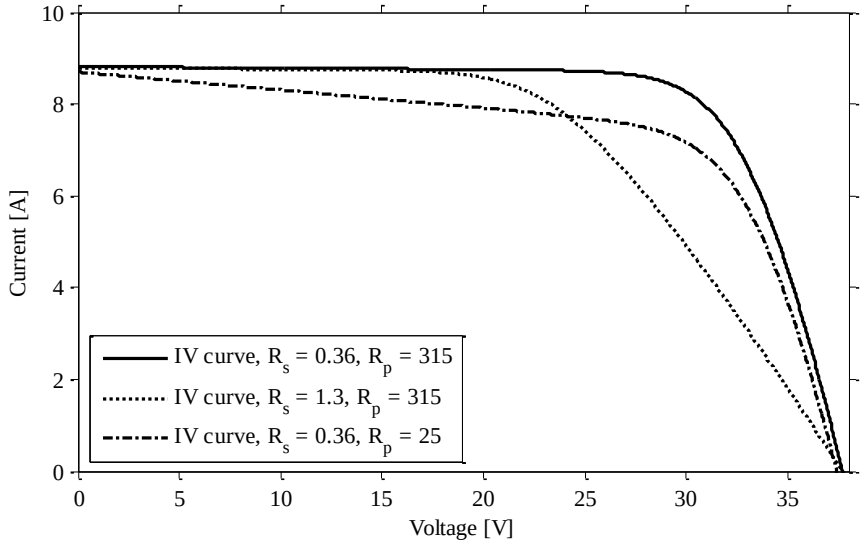

Figure 9: Modeled IV-curves illustrating the effects of R_s and R_p. The solid curve is a modeled IV-curve for the PV panel Windon Tatu 255 Multi.

In Figure 9 it can be observed that an increase of R_s results in a decreased voltage for the same current in the rightmost part of the curve. This decrease in voltage can be explained by analyzing the equivalent circuit in Figure 7 where an increased R_s leads to an increased voltage drop over R_s for the same current, thus leading to a decreased output voltage. Furthermore, a decrease in R_p leads to a decreased current for the same voltage in the leftmost part of the curve. This decrease in current can be explained by analyzing the equivalent circuit in Figure 7, where a decrease in R_p will lead to higher I_{R_p} for the same voltage. As the total photon generated current I_L is divided between I_D, I_{R_p} and I_{out}, and I_D remains constant whilst I_{R_p} increase, there will be a decrease in I_{out}.

4.2 Equivalent model for a photovoltaic panel

To model the behavior of a PV panel, the *one diode model equation* is used [14]. The equation can, according to [17], be derived from the *one diode model* in Figure 7 in combination with (2) according to

$$I_{out} = I_L - I_0 \cdot (e^{\left(\frac{V_{out}+I_{out}\cdot R_S}{N\cdot n\cdot V_t}\right)} - 1) - \frac{V_{out} + I_{out} \cdot R_s}{R_p}. \quad (4)$$

By sweeping the voltage, V_{out} in (4), an IV-curve is produced, see Figure 8. In this project a specific PV panel is modeled, the Windon Tatu 255 Multi. Data for this panel was provided by the Technical Research Institute of Sweden, SP, and is summarized in Table ***2*** and Table 3. Except for this data, high resolution IV-curves for the three different irradiances found in Table ***2*** were provided.

Table 2: Data from PV industry standard tests on the PV panel Windon Tatu 255 Multi, provided by SP.

Irradiance [W/m^2]	I_{sc} **[A]**	V_{oc} **[V]**	I_{MPP} **[I]**	V_{MPP} **[V]**	P_{MPP} **[W]**
1000 W/m^2	8.815	37.729	8.234	30.097	247.831
800 W/m^2	7.089	37.352	6.595	30.247	199.466
600 W/m^2	5.286	36.886	4.955	30.288	150.059

Table 3: Data from PV industry standard tests on the PV panel Windon Tatu 255 Multi, provided by SP.

R_s	0.36	(60 cells) x (0.06 Ω/cell)
dV/dI at I_{sc}	315	Average for the three measured irradiances.
dV/dI at V_{oc}	0.56	Average for the three measured irradiances.

The parameters I_0, n, I_L, R_s and R_p in (4) are PV panel specific, and must be known to generate an IV-curve. The parameter R_s is stated in Table 3. An approximation of R_p is the derivative of the voltage with respect to current at the short circuit operating point, which is also given in Table 3 [21] [22]. Furthermore, I_L can be calculated using I_{sc} from Table ***2*** when R_s and R_p are known. Though, the parameters n and I_0 are not given.

A method to find n and I_0 is presented in Section 4.3 [23]. Furthermore, as a first step towards an accurate IV-curve model, a model with moderate fit is constructed in Section 4.4.1. This is done to simplify the understanding of the procedure to construct an IV-curve with close to accurate fit in 4.4.2. A method to extract the parameters I_0, n, R_s and R_p by using only a measured IV-curve (i.e. without the data in Table 3) is presented in Section 4.4.3. By using the method in Section 4.4.3 it is, to a certain extent, possible to verify if dV/dI at I_{sc} is a good approximation of R_p. This parameter validation will be performed last in Section 4.4.4.

4.3 Identification of ideality factor and saturation current

To produce an IV-curve model from (4), the ideality factor n and the saturation current I_0 is required. A method to find these parameters is described in [23] and demonstrated in this Section using equations (5) - (12).

By assuming $I_D \gg I_0$, (2) can be approximated according to

$$I_D = I_0(e^{\frac{V_D}{N_c n V_t}}). \quad (5)$$

To simplify (5), C_{diode} is introduced as

$$C_{diode} = \frac{1}{N_c \cdot n \cdot V_t} \tag{6}$$

and (5) can now be written as

$$I_D = I_0 e^{C_{diode} \cdot V_D}. \tag{7}$$

The significant operating points for the PV panel modeled in this project are presented in Table **2**. These operating points, in combination with (6) and (7), can be used to find values for I_0 and n. In Sections 4.4.2 and 4.4.3 methodologies are presented where modeled IV-curves are created that have close to accurate fits to the measured IV-curves. However, to simplify the calculations and better explain the methodologies, IV-curve model parameters that generate curves with moderate fits are found in this Section as a first step. To find I_0 and n that give a model with a moderate fit, it is assumed that $R_s = 0$ and $R_p = \infty$. An analysis of the circuit in Figure 7 then gives that, at no load conditions, $V_D = V_{oc}$. Furthermore, at no load $I_D = I_L$, as both I_{Rp} and I_{out} are zero. In addition, $I_L = I_{sc}$ at short circuit conditions. Since I_L is constant for all load conditions (at a specific irradiance), $I_D = I_{sc}$ at no load. With known values of I_D and V_D at no load, two parameters remain unknown in (7), C_{diode} and I_0. To find these parameters, another analysis of the circuit in Figure 7, but with evaluation at MPP, can be conducted. This analysis gives $I_D = I_L - I_{MPP}$. As both I_L and I_{MPP} are known, I_D can be calculated. Also, at the MPP it is known that $V_D = V_{MPP}$. Now, using (7), an equation for the no-load condition can be formulated according to

$$I_{SC} = I_0 e^{C_{diode} \cdot V_{OC}}. \tag{8}$$

and an equation for the MPP operating condition can be formulated according to

$$I_L - I_{MPP} = I_0 e^{C_{diode} \cdot V_{MPP}}. \tag{9}$$

By combining (8) and (9), C_{diode} can be expressed as

$$C_{diode} = \frac{e^{(I_L - I_{MPP})} - e^{I_{SC}}}{V_{MPP} - V_{oc}}. \tag{10}$$

By using C_{diode}, (6) can be rewritten as

$$n = \frac{q}{N_c \cdot C_{diode} \cdot k_b \cdot T} \tag{11}$$

to calculate n. Furthermore, by combining (8) and (9), I_0 can be expressed as

$$I_0 = \frac{I_{SC}}{e^{C_{diode} \cdot V_{OC}}}. \tag{12}$$

4.4 IV-curve modeling

This Section describes the procedure to create a modeled IV-curve that fits to the measured IV-curve of the PV panel Windon Tatu 255 Multi. Then, in Section 4.4.4, it is concluded which IV-curve model to use in further analyses in the project.

4.4.1 Modeling an IV-curve with moderate fit

By using the significant operating points from Table *2* to calculate the parameters n and I_0, as described in Section 4.3, (4) can be used to create a IV-curve model. The process is described in a flow chart in Figure 10.

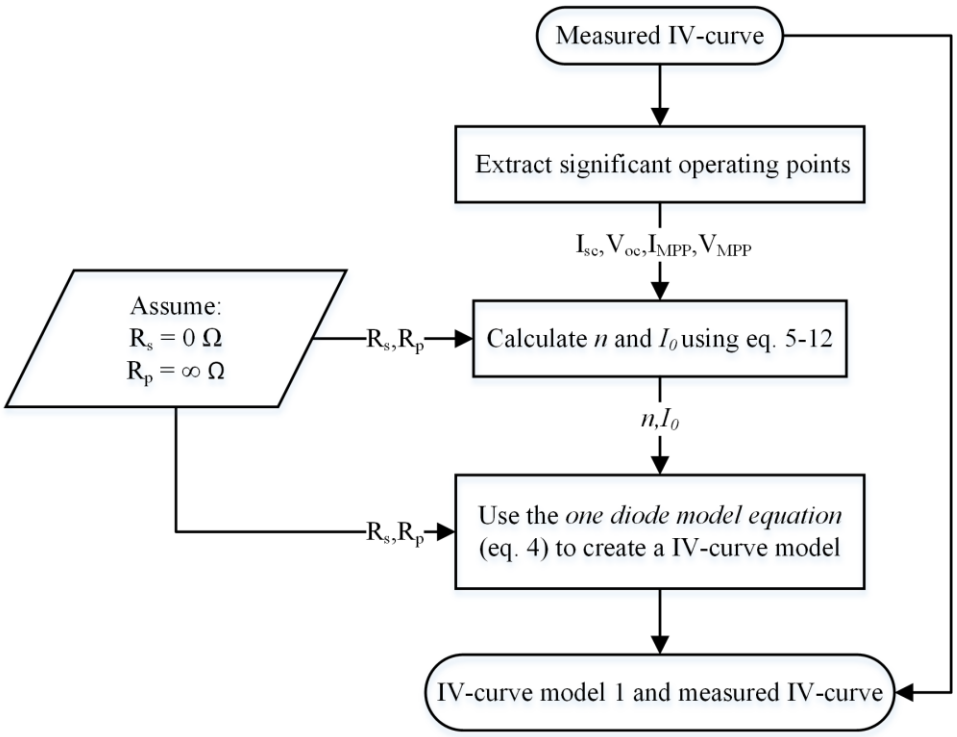

Figure 10: Flow chart describing the process of constructing a modeled IV-curve with moderate fit.

Figure 11 presents the modeled IV-curve created by using the process described by the flow chart in Figure 10. This IV-curve model is denoted IV-curve model 1 and its parameters are presented in Table 5 in section 4.4.4. Also present in Figure 11 is the measured IV-curve at 1000 W/m^2 for comparison. All modeled IV-curves in this project are generated with MATLAB and its built in simulation environment SIMULINK [24]. Matlab codes are found in Appendix V.

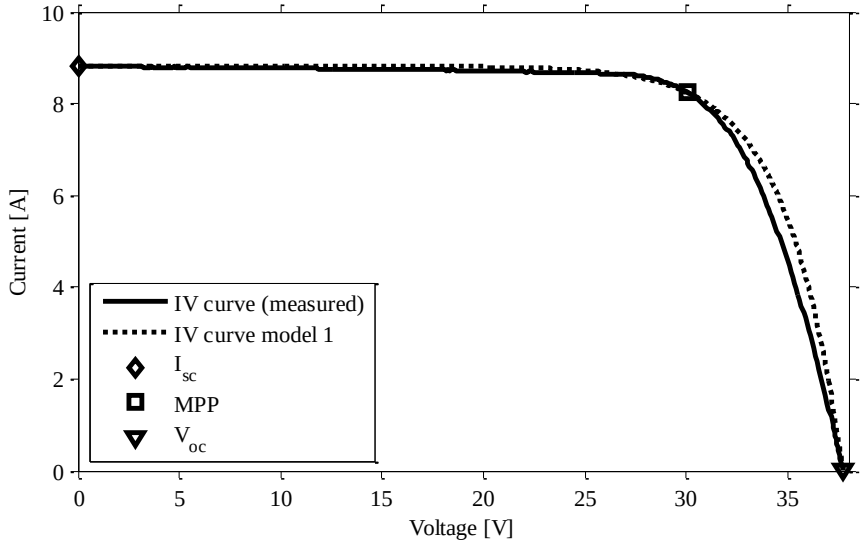

Figure 11: Measured and modeled IV-curves for the PV panel Windon Tatu 255 Multi at an irradiance of 1000 W/m^2. Significant operating points are indicated.

From Figure 11 it can be observed that the modeled and measured IV-curves differ slightly in between the significant operating points. Though, the curves intersect at the significant operating points. It can be concluded that the model roughly fits the measured curve. To improve the model, it has to be taken into consideration that $R_s = 0.36\ \Omega$ and $R_p = 315\ \Omega$, see Table 3. These resistances will affect the parameters n and I_0 as well as (4) and gives a more accurate IV-curve model, see Figure 14 in section 4.4.2.

4.4.2 Modeling an IV-curve with close to accurate fit

To construct a more accurate IV-curve model, R_s and R_p need to be taken into consideration both when n and I_0 is calculated and when (4) is used to model the curve. When calculating n and I_0 using (5)-(12) in 4.3, the significant operating points are used. Though, these operating points are affected by R_s and R_p and to understand how, an analysis of the circuit in Figure 7 is conducted.

Starting with the short circuit operation, a small current, I_{Rp}, will flow through R_p. As stated previously, a good approximation of R_p is the derivative of the voltage with respect to current at the short circuit operating point on the IV-curve [21], [22]. Thus, Table 3 gives that $R_p \approx 315\ \Omega$. Hence, at the short circuit operation point, I_{Rp} can be calculated as

$$I_{Rp} = \frac{I_{sc} \cdot R_s}{R_p} = 9\ mA. \tag{13}$$

At the open circuit operating point $V_D = V_{oc}$ and neither of the resistances affect this operating point. At the MPP, both R_s and R_p affect the operating point considerably. There will be a voltage drop over R_s, denoted $V_{Rs_{MPP}}$, that can be calculated as

$$V_{Rs_{MPP}} = I_{MPP} \cdot R_s = 2.96\ V. \tag{14}$$

The voltage over R_p at the MPP will be the sum of V_{MPP} and $V_{Rs_{MPP}}$, which results in a current, I_{Rp}, according to

$$I_{Rp} = \frac{(V_{MPP} + V_{Rs_{MPP}})}{R_P} = 0.1\ A. \tag{15}$$

A circuit, which is based on the circuit in Figure 7 but without the series and parallel resistances, is presented in Figure 12.

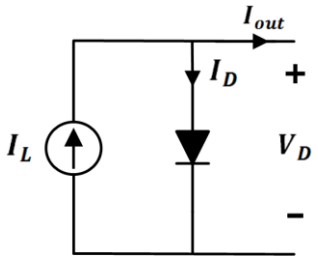

Figure 12: Modified circuit based on Figure 7, but without series and parallel resistances.

The circuit in Figure 12 represents a PV cell with no R_s and infinite R_p. By using the known values of the PV panel Windon Tatu 255 Multi from Table **2** and Table 3 together with (13)-(15), back-calculation can be performed which provides the output voltage and current that would be measured, if the panel had no R_s and infinite R_p. When back calculation is computed for the significant operating points, the values in Table 4 are obtained.

*Table 4: Data for modified significant operating points of the PV panel Windon Tatu 255 Multi. This data is assembled from Table 2 and Table 3 together with (*13)-*(15***)**.

Modified value	**Performed back-calculation**	**Equivalent parameter in Figure 12.**
$\boldsymbol{I_{sc}}$ (modified)	$I_{sc} + I_{R_p}$ = 8.824 A	I_{out} at short circuit.
$\boldsymbol{V_{oc}}$ (modified)	V_{oc} = 37.729 V	V_D at open circuit.
$\boldsymbol{I_{MPP}}$ (modified)	$I_{MPP} + I_{R_p}$ = 8.334 A	I_{out} at MPP.
$\boldsymbol{V_{MPP}}$ (modified)	$V_{MPP} + V_{D_{MPP}}$ = 33.057 V	V_D at MPP.

If these modified operating points are used when calculating n and I_0 according to the method described in Section 4.3 (eq. 5-12), new values for n and I_0 will be found (compared to those used for the IV-curve model 1 in Figure 10). Furthermore, if these new values for n and I_0 are used in (4) in combination with R_s and R_p equal to 0.36 Ω and 315 Ω respectively, a new IV-curve model can be generated, denoted IV-curve model 2. The process is described in a flowchart, see Figure 13. IV-curve model 2 is presented in Figure 14 together with the measured IV-curve.

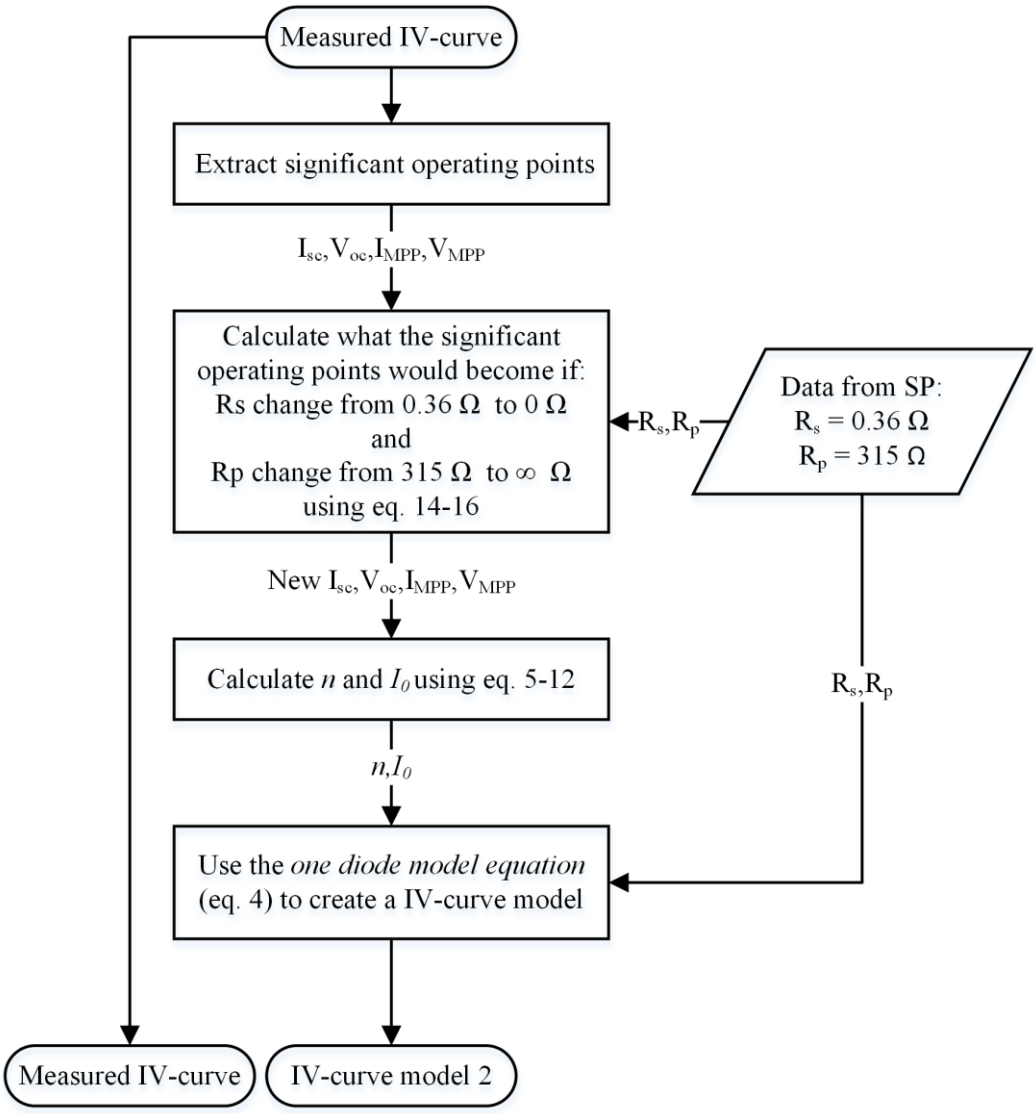

Figure 13: Flowchart describing the process of creating IV-curve model 2.

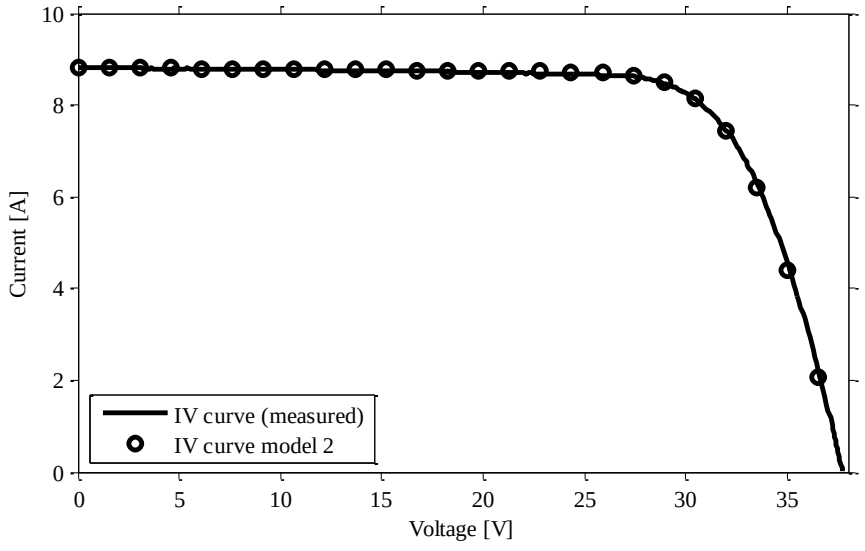

Figure 14: Measured and modeled IV-curves for the PV panel Windon Tatu 255 Multi at 1000 W/m^2 irradiance.

From Figure 14 it can be observed that IV-curve model 2 has a close to accurate fit to the measured IV-curve of the PV Panel Windon Tatu 255 Multi. Thus the method of using back-calculation proves to give a satisfactory result.

4.4.3 Finding an IV-curve model through parameter iteration

When using the *one diode model equation* (eq. 4) to generate an IV-curve model that fits a measured IV-curve, correct values for R_s, R_p, n and I_0 are required. If the only data available is the measured IV-curve, a different method can be used to iteratively find the required model parameters. It builds upon the methods presented in Sections 4.3, 4.4.1 and 4.4.2, but as a final step it uses the residual sum of squares (RSS) to detect if the parameters used give an accurate fit. The method is described in a flowchart, see Figure 15.

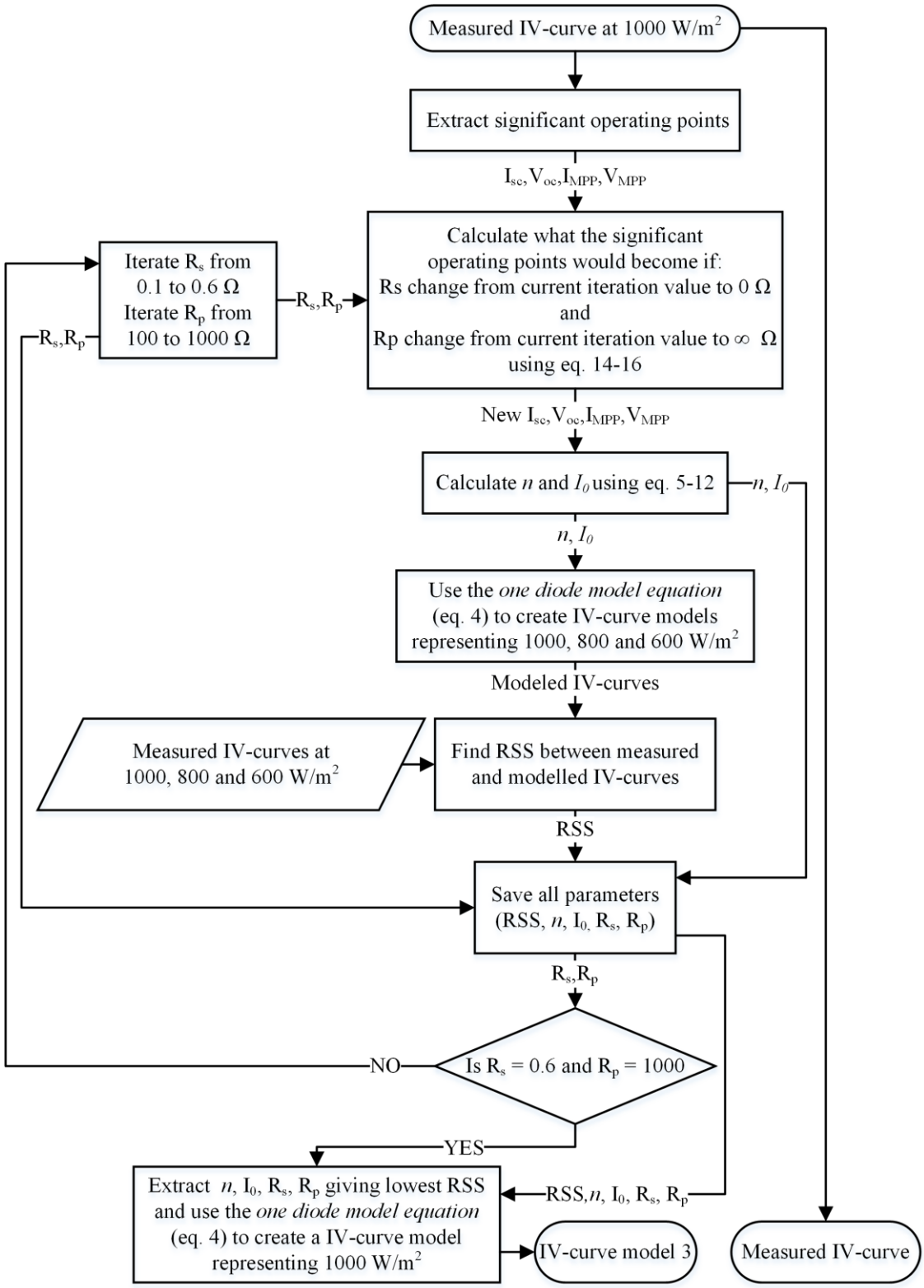

Figure 15: Flowchart describing the method of constructing IV-curve model 3 that fits the measured IV-curve well.

In the method described in Figure 15, R_s and R_p are iterated from 0.1 Ω to 0.6 Ω and 100 Ω to 1000 Ω respectively. This is to cover a broad interval of resistance values to find the best fit. R_s is iterated with a step size of 0.01 Ω and R_p at a step size of 5 Ω. By calculating which combination

of R_s and R_p (giving a certain n and I_0) that results in a modeled IV-curve which in total deviates the least from the measured IV-curves, a best fit can be found. The method can be simplified by only comparing one modeled and one measured IV-curve, but as three measured IV-curves at different irradiances were provided, a best fit to all three curves was performed. To find the deviation between modeled and measured curves, RSS was used. RSS is defined as

$$RSS = \sum_{i=1}^{n} (y_i - f(x_i))^2 \tag{16}$$

where y_i is the measured value and $f(x_i)$ is the corresponding model value [25]. The RSS is therefore a sum of squared errors. When the iteration of R_s and R_p are completed, the model parameters that give the best fit can be determined. The parameters used in the IV-curve model generated according to the process described in Figure 15 are presented in Table 5 in Section 4.4.4. Moreover, conclusions regarding which IV-curve model to use in further modeling are also presented in Section 4.4.4.

4.4.4 Conclusions regarding modeled IV-curves

The parameters used in the IV-curve models generated in Sections 4.4.1, 4.4.2 and 4.4.3 are presented in Table 5. Furthermore, the method described in the flowchart in Figure 15 can, to some extent, be used to verify if dV/dI at I_{sc} is a good approximation of R_p, as stated in the Section 4.2. This verification can be performed by assuming R_s = 0.36 (from Table 3) and only iterate R_p until a best fit is found. R_p and the corresponding model parameters for such best fit are also presented in Table 5, denoted IV-curve model 4.

Table 5: Summary of parameters for IV-curve models evaluated throughout chapter 4.

IV-curve model	R_s	R_p	n	I_0	RSS 1000W/m^2	RSS 800W/m^2	RSS 600 W/m^2	RSS Total
IV-curve model 1	0	∞	1.8196	$1.2756 \cdot 10^{-5}$	71.18	6.48	36.13	113.79
IV-curve model 2	0.36	315	1.0369	$4.9907 \cdot 10^{-10}$	3.30	0.47	0.25	4.02
IV-curve model 3	0.32	260	1.0932	$1.6847 \cdot 10^{-9}$	0.53	0.43	0.34	1.30
IV-curve model 4	0.36	235	1.0100	$2.6617 \cdot 10^{-10}$	2.27	0.32	0.58	3.17

From Table 5 it can be concluded that the best total fit is achieved by using the iterative method described in Section 4.4.3, giving IV-curve model 3. Consequently, it can be concluded that the iterative method described in Section 4.4.3 can be used to find a well-fitting model for an arbitrary PV panel with known IV characteristics. Though, the model was only compared with three measured IV-curves. A comparison with additional measurement data could increase the credibility of the method, if it would still give the best fit. However, as industry standard equipment was used to determine R_s to be 0.36 Ω, see Table 3, this value will be used in further modeling in this project. When R_s was set to 0.36 Ω and R_p was iterated, it was found that when R_p was 235 Ω (IV-curve model 4), a slightly better fit was accomplished compared to the previously assumed 315 Ω. Therefore R_p is set to 235 Ω in further modeling in this project. A comparison between IV-curve model 4 and the measured IV-curves is presented in Figure 16.

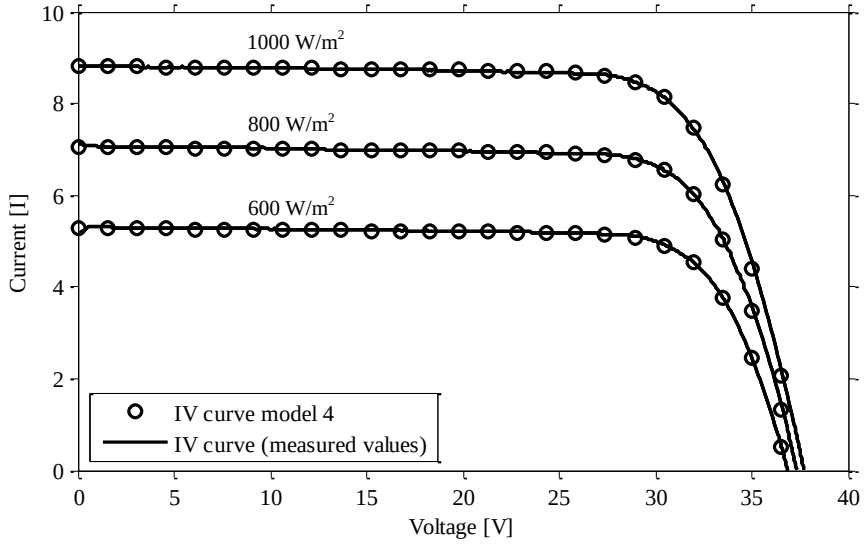

Figure 16: Comparison between IV-curve model 4 and measured IV-curves for irradiances 1000 W/m^2, 800 W/m^2 and 600 W/m^2. The modeled IV-curves fit well to the measured IV-curves.

It can be concluded that IV-curve model 4, with model parameters specified in Table 5, fits well to the measured IV-curves.

5 Modeling of maximum power point tracker

There are many different MPPT algorithms. In [10] an overview of over 90 research papers on MPPT techniques is presented. From the survey, 19 distinct MPPT methods are identified and presented. One of the presented methods is implemented in this project; the incremental conductance (or IncCond) method.

5.1 The IncCond method

The main reasons to choose the IncCond method include that:

- It is described in 11 of the 90 papers in [11]. Most other methods are described in fewer papers. This indicates that the IncCond method is relatively common.

- It is relatively simple to implement, with straightforward mathematics and logic describing the method.

- It can be implemented using a microcontroller which allows for control using simple digital logic, like if and else statements. In addition, with some minor modifications, the method can be implemented using proportional integral (PI) control [11], which gives added flexibility in the implementation. A short description of IncCond implementation using a PI controller is found in Appendix III.

- The convergence speed is variable, giving high flexibility. Especially when power smoothing is to be introduced in the control strategy, a variable convergence speed is important (see Section 6.1).

- The technique does not require periodic tuning, which means that the MPPT will keep its efficiency over time even if the PV system is degraded or if other site specific conditions change.

The IncCond method uses the fact that the PV-curve (see Figure 8) has a maximum for every irradiance level. On the left of the maximum, the slope of the PV-curve is positive and on the right side the slope is negative. At the maximum, the slope is zero. Mathematically this can be expressed as

$$\begin{aligned} \frac{dP}{dV} &= 0 && \text{at MPP} \\ \frac{dP}{dV} &> 0 && \text{left of MPP} \\ \frac{dP}{dV} &< 0 && \text{right of MPP.} \end{aligned} \tag{17}$$

The derivative of the PV-curve, dP/dV, can be expressed as

$$\frac{dP}{dV} = \frac{d(IV)}{dV} = I \cdot \frac{dV}{dV} + V \cdot \frac{dI}{dV} = I + V\frac{dI}{dV} \approx I + V\frac{\Delta I}{\Delta V} \tag{18}$$

and (18) can be rewritten as

$$\frac{dP}{dV} = \ I + V\frac{\Delta I}{\Delta V} \Rightarrow \frac{(dP/dV)}{V} - \frac{I}{V} = \frac{\Delta I}{\Delta V}. \tag{19}$$

For $V > 0$, (17) and (19) gives

$$\begin{aligned} &\frac{\Delta I}{\Delta V} = -\frac{I}{V} && \text{at MPP} \\ &\frac{\Delta I}{\Delta V} > -\frac{I}{V} && \text{left of MPP} \\ &\frac{\Delta I}{\Delta V} < -\frac{I}{V} && \text{right of MPP.} \end{aligned} \tag{20}$$

By frequently comparing the instantaneous conductance (I/V) with the incremental conductance ($\Delta I/\Delta V$), the MPP can be tracked. The flowchart in Figure 17 describes how IncCond, by means of if and else statements, is implemented [10].

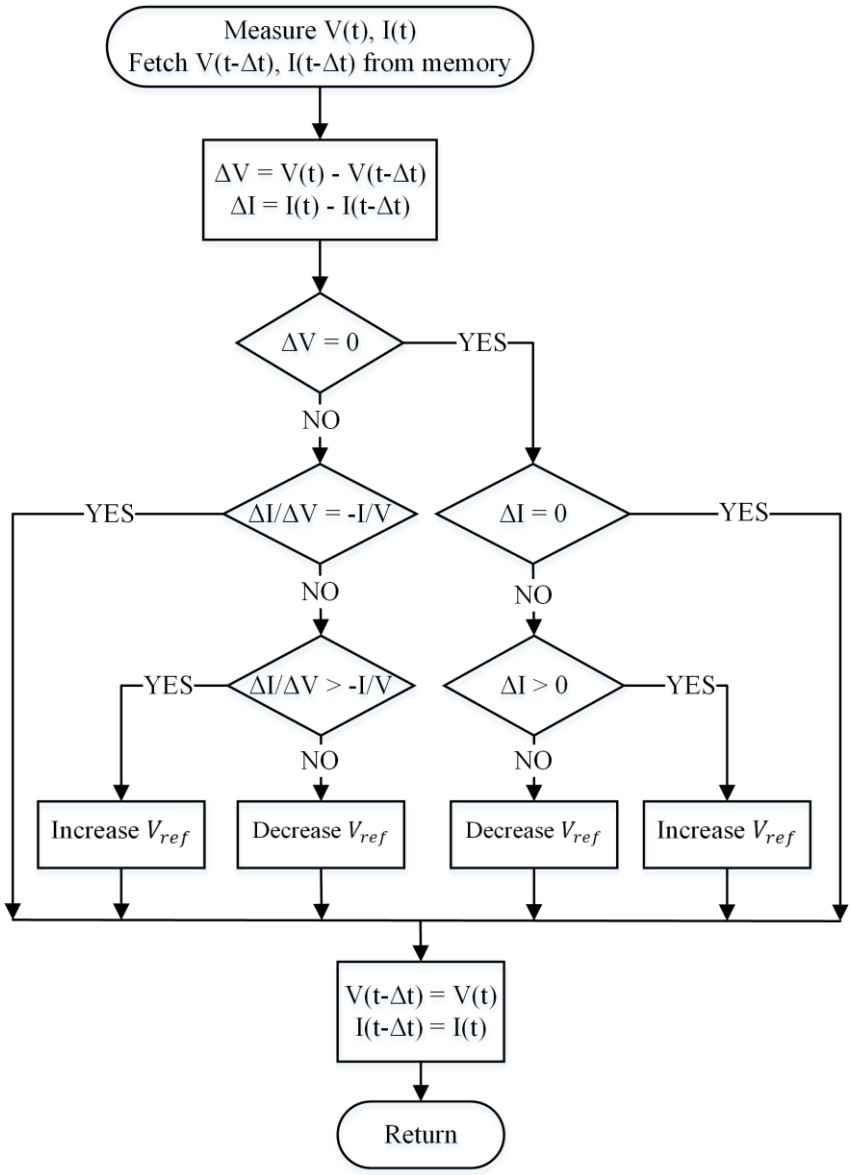

Figure 17: Flowchart describing the IncCond MPPT algorithm [10].

In Figure 17 the inputs are measured current and voltage from the PV panel(s). The IncCond method requires that the previous voltage and current are kept in memory between each iteration in order to calculate the incremental conductance. Depending on the relation between the previous and present current and voltage, a new voltage reference, V_{ref}, will be the output of the controller. The PV panel(s) will be forced to operate at V_{ref}, resulting in new current and voltage inputs to the controller at the next iteration. More frequent iteration and larger increment/decrement of V_{ref} give a faster controller. However, the latter will result in more oscillation around the MPP as larger steps in voltage close to the MPP result in lower probability to end up at, or close to, the MPP.

5.2 Validation of MPPT functionality

In order to validate the MPPT functionality, irradiance test signals were supplied to a simplified PV system model. More on the PV system modeling is found in Section 7.2. The test signals help

to clarify the MPPT behavior for certain well defined inputs, which simplifies the identification of irradiance changes that might constitute a problem for the MPPT algorithm. The test signals used include step change, ramp, triangular and sinusoidal signals.

The step change signal is used to illustrate that the MPPT does not necessarily need to change the reference voltage to operate close to the MPP after a rapid irradiance increase. This is because of the characteristics of the IV-curve. This fact is important to consider when designing a smoothing algorithm, see Chapter 6, as it emphasize the need for the smoothing algorithm to be active during a rapid irradiance increase. Only deactivating the MPPT will not achieve a satisfactory smoothing functionality.

The ramp and triangular test signals are used as they are standard signals for testing MPPT functionality according to the European standard prEN 50530 [26]. In this standard, there are specific ramp rates and amplitudes stated for the test signals. The highest ramp rate (continuous) in the standard is 100 W/m^2/s and the highest amplitude is 700 W/m^2. A higher maximum ramp rate is found in the logged irradiance data, 573 W/m^2/s ($Irr_{deriv,max}$). It is reasonable to assume that that a higher ramp rate makes it more difficult for the MPPT to track the MPP. Therefore this higher ramp rate is used for the test signals in order to illustrate any potential MPPT algorithms' weakness. Also a higher amplitude, 982 W/m^2 ($Irr_{max,30}$), is used for the test signals instead of that used in the standard. This is because test signals with higher amplitude can better evaluate the smoothing algorithm, see Chapter 7, and it is convenient to test the MPPT using the same test signals. The latter simplifies the comparison between the power outputs when using smoothing verses using only the MPPT. Also, an advantage of using higher amplitude in the test signal is that the MPPT functionality is evaluated over a wider range of the PV panels' operating range. The sinusoidal test signal means to mimic the characteristics of irradiance variations. The maximum derivative in the sinusoidal test signal is set to $Irr_{deriv,max}$. For all test signals the lowest irradiance used is 100 W/m^2 due to that none of the maximum irradiance differences within 30 seconds found in April, see Section 3.4, reached below this irradiance level.

In theory, the update rate of the MPPT algorithm should be set as fast as possible to achieve the fastest possible MPP tracking accuracy. However, practically the update rate is limited by the processing power of the microcontroller used for implementation. In this project, the smoothing algorithm is designed to work together with the MPPT algorithm, see Chapter 7, and the two algorithms have proved to work well together when they use the same update rate. No configuration using different update rates for the two algorithms has been tested. The limit for the update rate of the MPPT is therefore set by the smoothing algorithm, which requires more processing power. This is because the smoothing algorithm saves multiple values in a buffer at each iteration. In addition, it is assumed that implementation of the smoothing algorithms may be simplified if it runs on the same microcontroller and with the same update rate as the MPPT algorithm. It was found that an operation at 400 Hz (corresponding to a simulation time-step of 0.0025 s/S) results in a satisfactory tracking accuracy and smoothing functionality as well as a reasonable simulation time.

The voltage step-size in the MPPT is set to 0.25 V/step. This setting was found by iteration and it gives a satisfactory balance between voltage, current and power variations when the test signals

are applied and during steady state operation. Steady state operation in this project is defined as operation during a constant irradiance of 1000 W/m^2 (which is the irradiance used at standard test conditions, STC, for PV panels). In steady state a smaller step-size is desirable, as it reduces the voltage and current variations and thus the power variations. Though, the speed of the MPPT is reduced if the voltage step-size is lowered. Also, the voltage fluctuations are increased significantly during the positive irradiance change of the ramp and triangular test signals if the step-size is decreased. The reason for this behavior is that the increase in irradiance results in a significant increase in current, and even though the voltage is lowered by 0.25 V at each iteration during multiple iterations, the resulting power change, $\Delta P = \Delta U \cdot \Delta I$, is still increased due to the increase in current. This increase in power is interpreted by the MPPT algorithm as if a continuous decrease in voltage drives the operating point closer to the MPP, thus the decrease of the voltage reference continues. Though, this misinterpretation stops when the voltage becomes low enough to cause a lowering in power from one iteration to the next. When this occurs, the voltage starts to increase again. A larger voltage step-size allows the MPPT algorithm to faster detect that the operating point is driven away from the MPP, as the decrease in voltage at each iteration then becomes the more dominant factor when ΔP is calculated. In Table 6 the maximum voltage deviations during ramp test irradiance signal and steady state operation for different step-sizes are presented. In addition to affect the performance of the MPPT algorithm, the step-size also has an effect on the performance of the smoothing algorithm, as the two algorithms are designed to operate together (see Section 6.1). The smoothing algorithm is found to operate satisfactorily together with the MPPT when the step-size is 0.25 V.

Table 6: Maximum voltage deviations during ramp and steady state operation for different step-sizes when the MPPT algorithm is used.

Voltage step-size [V]	Max voltage deviation from optimal during ramp test irradiance signal [V]	Steady state deviation from optimal [V]
0.1	11.3	0.2
0.25	6.5	0.5
0.5	3	1

To evaluate the performance of the MPPT, an analysis of the modeled PV panel's maximum power and optimal voltage and current for a range of irradiance levels was conducted. The irradiance was swept from 0.2 W/m^2 to 1300 W/m^2 in steps of 0.2 W/m^2. At each irradiance level, the maximum power and the corresponding voltage and current was evaluated. The result is shown in Figure 18.

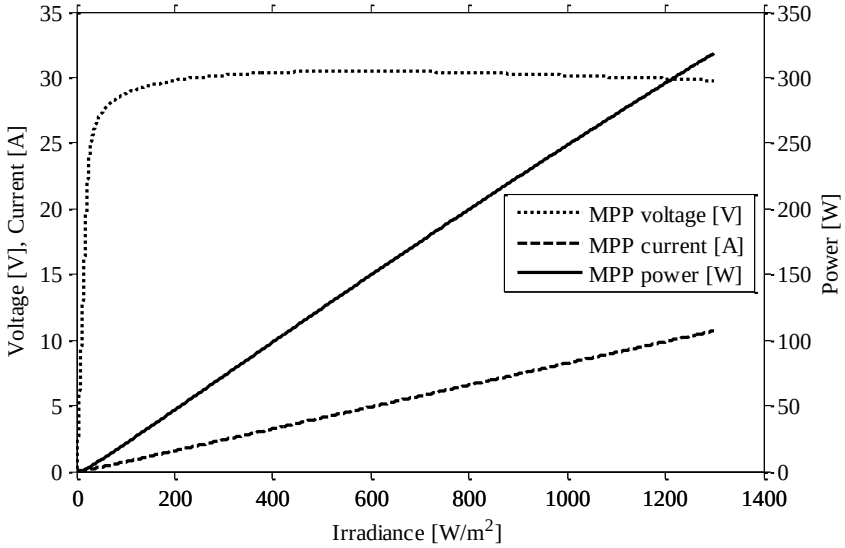

Figure 18: Maximum power, optimal voltage and optimal current outputs as a function of irradiance.

The power- voltage- and current outputs when MPPT is used are compared with the optimal values from Figure 18. The optimal characteristics together with the MPPT output characteristics during the triangular- and sinusoidal test signals are presented in Figure 19. The same characteristics for step- and ramp test signals are found in Appendix III.

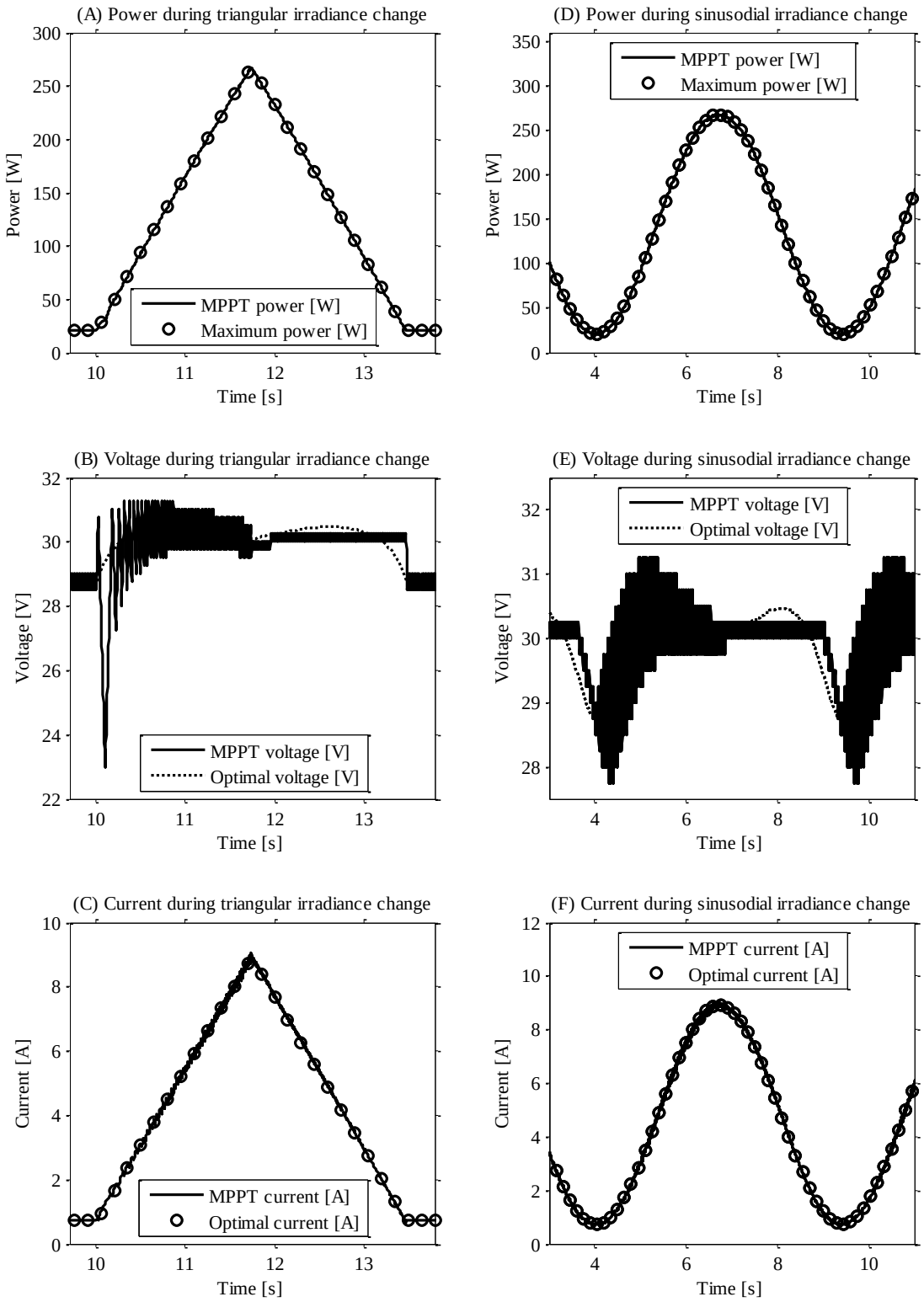

Figure 19: Power, voltage and current output from the MPPT when irradiance test signals are applied. In A, B and C, the power, voltage and current during a triangular irradiance test signal are illustrated. The same entities are presented in D, E, and F, but for a sinusoidal irradiance test signal.

In Figure 19 A, it can be observed that the MPPT power and maximum possible power is similar. However, the MPPT power deviates slightly from the maximum power just after the triangular irradiance signal is applied. This is, as can be observed in Figure 19 B, due to the voltage

variations at this time. The voltage variations are caused by the MPPT algorithm misinterpretation described previously in this Section. The current seen in Figure 19 C is close to the optimal current, though some small variations can be observed when the irradiance increases due to the voltage variations. During the sinusoidal test signal in Figure 19 D, it can be observed that the MPPT power and the maximum possible power are close to each other. Some voltage variations are observed in Figure 19 E. This is due to the same MPPT algorithm misinterpretation that causes the voltage variations in Figure 19 B. The current in Figure 19 F is close to the optimal, though similar small variations as in Figure 19 C can be observed, due to the voltage variations. Overall, it can be concluded that the MPPT works satisfactorily in terms of MPP tracking, and reasonably regarding the operation at the optimal voltages and currents. The sign of the voltage- and current variations are opposite to each other most of the time during the irradiance increase for both the triangular and sinusoidal test signals. This is why these variations are not reflected in the power.

6 Power smoothing of photovoltaic power output

To smooth the output power from the PV system, a *smoothing algorithm* was developed. The smoothing algorithm is designed to run on a microcontroller, same as for the MPPT algorithm. This simplifies the implementation of both the MPPT and smoothing functionalities, as both algorithms can run on the same microcontroller.

The smoothing algorithm is designed to activate when a positive power increase from the PV system exceeds a certain limit, the *maximum allowed ramp rate* (W/s). When the rate of change in power is no longer exceeding the maximum allowed ramp rate, the smoothing algorithm is deactivated and the MPPT algorithm is activated.

6.1 Design of power smoothing algorithm

Similar to the MPPT algorithm, the smoothing algorithm is designed to control the voltage from the PV system. Though, instead of tracking the MPP, the smoothing algorithm tracks the operating point that allows for the power increase to stay below a specified maximum allowed rate. By studying the IV-curve and PV-curve in Figure 8, two ways of limiting the power can be identified. Assuming initial operation at MPP, the voltage can either be increased or decreased to limit the power. The latter requires a large voltage decrease to accomplish a power limitation. This is difficult to achieve in a fast yet controlled way. Also, operating at a low voltage could limit the amount of systems that can use the smoothing algorithm, as a minimum voltage level is required for the PV system to operate [27]. In addition, the current will be high during the smoothing if the voltage is lowered significantly, which introduces additional heat in the PV panels and thus reduces their efficiency. Furthermore, high current and heat might stress the PV system components in general. Though, an advantage with power limiting using voltage reduction is that the power variations can be kept relatively low during smoothing without further measures, as a change in voltage will not cause a large change in power.

To keep operation relatively close to the V_{MPP}, to have low current levels and to achieve fast power limitation during smoothing, the smoothing algorithm was designed to increase the voltage when limiting the power. A flowchart of the suggested smoothing algorithm is presented in Figure 20.

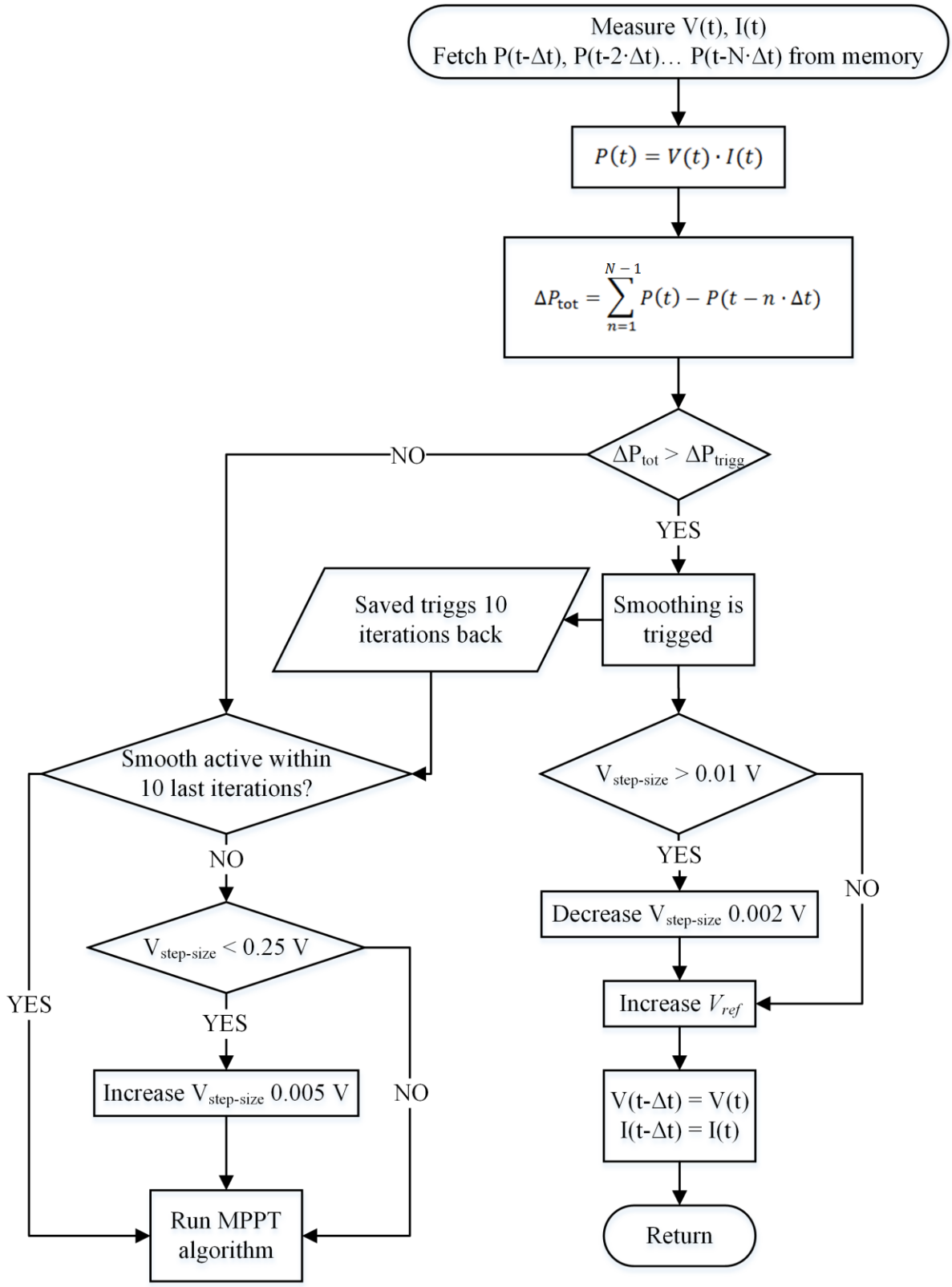

Figure 20: Flowchart describing the smoothing algorithm.

The smoothing algorithm uses voltage and current as input, same as the MPPT algorithm. The voltage and current are multiplied to get the instantaneous power. Furthermore, a certain amount of previous power levels are saved. The smoothing algorithm compares the instantaneous power

with previous power levels to detect if the maximum allowed ramp rate is exceeded. This is done in a way that reduces power variations during smoothing as well as allows for fast detection of a power increase caused by an irradiance increase.

To detect if the maximum allowed ramp rate is exceeded, the smoothing algorithm uses the sum of the differences between the instantaneous power and previous power levels. This sum is defined as

$$\Delta P_{tot} = \sum_{n=1}^{N-1} (P_{now} - P_n) \tag{21}$$

where P_n is the power n iterations before the present iteration in the algorithm and $N-1$ is the total number of summed power differences. The algorithm uses the fact that if all the power levels $N-1$ iterations before the present iteration and all power levels after the present iteration form a linear distribution with the positive ramp rate k (W/sample), ΔP_{tot} will have a constant value at each iteration, denoted ΔP_{trigg}. For example, if $k = 1$, and $N = 6$, then $\Delta P_{tot} = 15$. Thus, if $\Delta P_{tot} \leq 15$, then $k \leq 1$ must be fulfilled. Again, this relation between ΔP_{tot} and k is only true if the power levels are linearly distributed with slope k. A close to linear distribution of power levels will occur if there is one algorithm, in this case the MPPT, that at each iteration strives at increasing the power faster than k, and another algorithm, in this case the smoothing algorithm, that at each iteration strives at limiting the power increase when ΔP_{tot} exceeds ΔP_{trigg}. By comparing ΔP_{tot} at a certain iteration with ΔP_{trigg}, the algorithm can decide if a power smoothing should be initiated at the next iteration. If $\Delta P_{tot} > \Delta P_{trigg}$, smoothing is activated resulting in an increase of V_{ref}. If $\Delta P_{tot} < \Delta P_{trigg}$, the MPPT algorithm is activated.

However, if the desired value for $k \neq 1$, ΔP_{trigg} has to be scaled in order to limit the power at ramp rate k. By letting ΔP_{tot} at $k = 1$ be denoted $\Delta P_{tot,k1}$, an expression for ΔP_{trigg} valid for any ramp rate is

$$\Delta P_{trigg} = \Delta P_{tot,k1} \cdot p_{scale} \tag{22}$$

where p_{scale} is a dimensionless scaling factor which should have the same value as the maximum desired ramp rate, k. The expression for ΔP_{trigg} in (22) can be understood by studying (21). If $p_{scale} = 1$, ΔP_{tot} in (21) will be equal to $\Delta P_{tot,k1}$. If $\Delta P_{tot,k1}$ is scaled with a factor p_{scale}, this will, due to linearity, be the same as scaling each power difference in (21), i.e. $P_{now} - P_1$, $P_{now} - P_2$ etc. with the factor p_{scale}, thus each power difference is allowed to be p_{scale} times the value it is when $k = 1$. For example, if $P_{now} - P_n$ is multiplied by 2 (i.e. p_{scale} = 2), this will allow for double the power increase between an iteration n samples back and the current iteration, compared to when $k = 1$. This is the same as going from allowing a ramp rate of 1 W/sample to 2 W/sample. Thus, (22) gives a value for ΔP_{trigg} that, if used in the smoothing algorithm, limit the ramp rate to k.

For convenience, the ramp rate can be expressed in W/s, and a conversion from W/s to W/sample is made according to

$$k = \frac{W/s}{samples/second} \tag{23}$$

where k has the unit W/sample.

However, the power does not always increase at ramp rate k, thus the relation $\Delta P_{tot} > \Delta P_{trigg}$ may not be a correct indication that power smoothing should be activated. During the first N samples of a smoothing sequence, there is a high probability that ΔP_{trigg} should have a different value from that calculated in (22) to ensure a maximum ramp rate of k. Though, the ramp rate will approach k during smoothing, as the power becomes more linearly distributed. In addition, small power variations are present in the output power as the voltage is changed in discrete steps. These power variations introduce a small error in the algorithm. By increasing N, this error can be reduced. As the algorithm is based on the assumption that the power is distributed linearly, a larger N will give a ΔP_{tot} (that represent a certain slope for the specified N), that represent a more averaged power slope.

The strategy when designing the smoothing algorithm is to use the ramp test irradiance signal and tune the algorithm parameters to achieve a desired continuous power ramp rate when the test signal is applied. The reason for designing the smoothing algorithm to work with the ramp test signal is that it is assumed that a constant (or close to constant) power before smoothing represent an average change in irradiance. The ramp rate and amplitude of the test signal is set to $Irr_{deriv,max}$ and $Irr_{max,30}$ respectively, see Section 3.4. The reason for setting the maximum ramp rate to $Irr_{deriv,max}$ is that it was found that the higher the irradiance derivative, the more difficult it is to smooth the power. This is partly because a higher derivative gives more voltage variations (see Figure 19 B) when the MPPT algorithm is active. As the smoothing algorithm operates together with the MPPT algorithm, these voltage variations also affect the smoothing functionality. If the voltage, during a rapid irradiance increase, lowers due to the previously described misinterpretation by the MPPT algorithm (see Section 5.2), and the smoothing algorithm is activated, the voltage may not increase fast enough to achieve the desired power limitation. This may result in a higher ramp rate than the maximum allowed, thus the smoothing might not be achieved fast enough. For this reason the maximum ramp rate found in the irradiance data is used in the test signal to ensure that a satisfactory smoothing functionality is achieved for all irradiance variations.

The reason for choosing a 30 seconds interval for $Irr_{max,30}$ is that this is the time than it takes for the frequency controlled disturbance reserve to be fully activated [12]. The frequency controlled disturbance reserve is a control mechanism used in the Nordic Power System to regulate the frequency when there is a deviation of more than 0.1 Hz from the nominal frequency. One of the main goals of this project is to improve frequency quality by means of power smoothing. An assumption was made that if the logged irradiance data is used as input to a PV system and if this PV system is connected to a power system having a frequency controlled disturbance reserve, one of the largest frequency deviations will occur at the time when $Irr_{max,30}$ occurs. By ensuring that the power output from the PV system, when applying a test signal of amplitude $Irr_{max,30}$, is ramped at a rate which result in a 30 seconds delay until the amplitude $Irr_{max,30}$ is reached, the

most severe frequency variations are assumed to be reduced. This ramp rate was found to be 6.227 W/m^2/s. Presumably other maximum ramp rates can be set to achieve improved frequency quality. Nevertheless, the ramp rate chosen in this project proves to improve the frequency quality (see Section 7.3).

To choose a reasonable value for N, two main aspects need to be considered. The first is that N should not be too low. This is because the error due to power variations will then be relatively large. Also, due to the power variations, a low N might at times trigger the smoothing algorithm even during steady state (when there is no irradiance change). As the smoothing algorithm is designed to not increase the $V_{step-size}$ if the smoothing has been activated within the last 10 iterations, the $V_{step-size}$ will never increase if N is too low. This will cause the MPPT to not operate as intended. In addition, a lower allowed ramp rate demands a higher N to avoid that $V_{step-size}$ never increase, as ΔP_{trigg} will then be lower. The second aspect to consider is that N should not be too high. A high N gives a slower algorithm, as more values has to be saved at each iteration. Also, a high N might cause the smoothing algorithm to not initiate fast enough during a rapid irradiance increase. The latter is because ΔP_{trigg} will have a relatively high value if N is high. The time it takes for the smoothing to activate is dependent on ΔP_{trigg}, as the condition for activating smoothing is $\Delta P_{tot} > \Delta P_{trigg}$. For the smoothing algorithm in Figure 20, a satisfactory value for N was found to be 60. This choice allows for a relatively fast smoothing algorithm, and a freedom to reduce the power ramp rate by half, without having the problem that $V_{step-size}$ never increase. All parameter values used in the smoothing algorithm are found in Table 7.

Table 7: Parameters used in the smoothing algorithm.

Parameter	Value
N	60
k	8.227 W/s
Minimum voltage step-size	0.01 V
Maximum voltage step-size	0.25 V
Change in $\boldsymbol{V_{ref}}$ step-size if smoothing is active	-0.002 V
Change in $\boldsymbol{V_{ref}}$ step-size if smoothing is not active	0.005 V
Simulation time-step	0.0025 s/step

Reasonable values for the maximum- and minimum voltage step-size as well as the change in V_{ref} step-size, have been found iteratively. The parameter values in Table 7 give a satisfactory result regarding power-, voltage- and current variations during smoothing as well as regarding response time for activation of smoothing. The reason for having a decreased V_{ref} step-size during smoothing is that the current variations would otherwise be large when the voltage is changed. This is because operation is above V_{MPP} during a power smoothing sequence, and the slope of the IV-curve is therefore relatively steep (see Figure 8). Furthermore, as can be seen in the flowchart in Figure 20, the smoothing algorithm is designed to not increase V_{ref} unless 10 iterations without the activation of the smoothing algorithm have passed. This is done to prevent the MPPT from changing the voltage more than the smoothing algorithm can do during a smoothing sequence. Without this delay, the ramp rate would become higher than the desired maximum ramp rate, as the MPPT would act in a more forceful way compared to the smoothing algorithm.

An important parameter in the smoothing algorithm is the simulation time-step. A smaller simulation time step allows the smoothing algorithm to limit the power ramp rate more forcefully. This is because more voltage changes can be achieved within the same time frame. A shorter simulation time-step therefore gives better controllability. The possibility to more forcefully limit the power is particularly important in the initial part of a smoothing sequence, when the voltage is usually close to the V_{MPP}. When the operation is close to MPP, a relatively large positive change in voltage is required to achieve a fast power limitation, compared to the operation at higher voltage levels.

6.2 Evaluation of the power smoothing algorithm

In Figure 21 the results from using smoothing on a ramp- and sinusoidal test signal are presented. The derivative of the ramp test signal and the maximum derivative of the sinusoidal test signal are $Irr_{deriv,max}$. The amplitude of the ramp and sinusoidal test signals is $Irr_{max,30}$. The IV characteristics of the modeled PV panel are used to represent the behavior of a PV system. In addition, the results of smoothing step- and triangular irradiance test signals are presented in Appendix III.

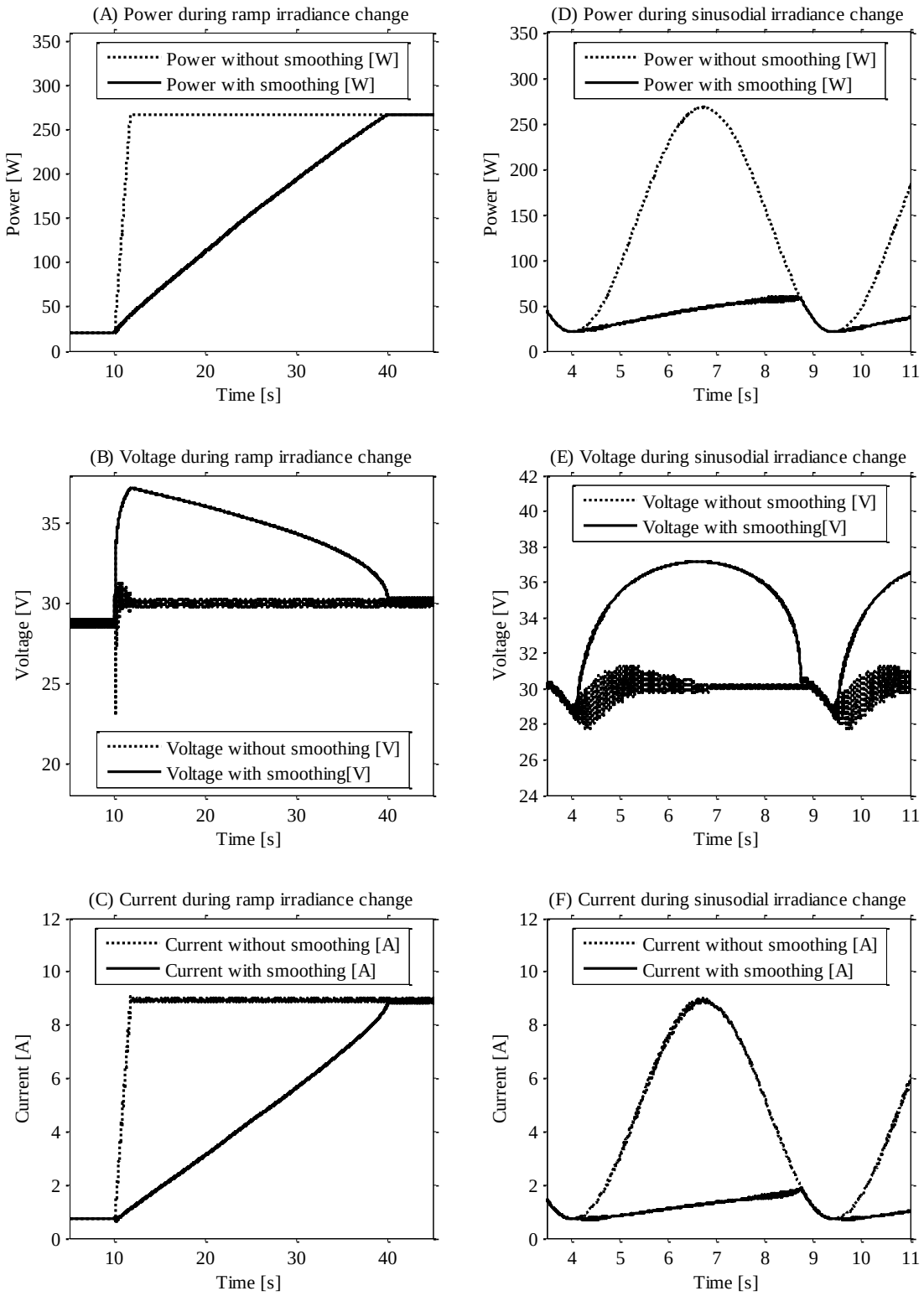

Figure 21: Power, voltage and current output from PV model with and without smoothing when ramp and sinusoidal test signals are applied.

In Figure 21 A it can be observed that the power is smoothed close to linearly for 30 seconds. The ramp rate is around 8.22 W/m^2/s. The smoothing algorithm was tuned using the ramp irradiance test signal, thus Figure 21 A confirms that the tuning resulted in a smoothed power output having the desired ramp rate. The voltage increases rapidly during the initial part of the applied irradiance

ramp in order to achieve a fast power limitation. In Figure 21 C it can be observed that the current is kept relatively low during smoothing due to the operation at high voltage. In Figure 21 D, E and F, the power, voltage and current during a sinusoidal test irradiance signal are illustrated when the smoothing algorithm and the MPPT algorithm are used. The ramp rate when smoothing is applied in Figure 21 C was found to be around 10 $W/m^2/s$. This is slightly higher than when smoothing the ramp test signal. The difference is probably due to that the irradiance is not the same for the two test signals just before the smoothing sequence starts. Also, there are small variations in the power output for a longer time during the smoothing of the sinusoidal test signal which introduce additional error. Like in Figure 21 C, the current in Figure 21 F is lowered when smoothing is applied due to operation at high voltage.

7 Modeling frequency behavior in an islanded power system

7.1 Modeling a hydro power plant

One of the main objectives of this project is to evaluate the effects on frequency quality when a PV system is connected to a simplified power system. The frequency quality in the power system is determined by the characteristics of the loads and power sources in the power system. One electric power source, which is common in Sweden, is hydro power [28]. Hydro power is used for bulk production of electricity as well as for frequency regulation. The block diagram in Figure 22 describes how a typical frequency control operates in a hydro power plant [29].

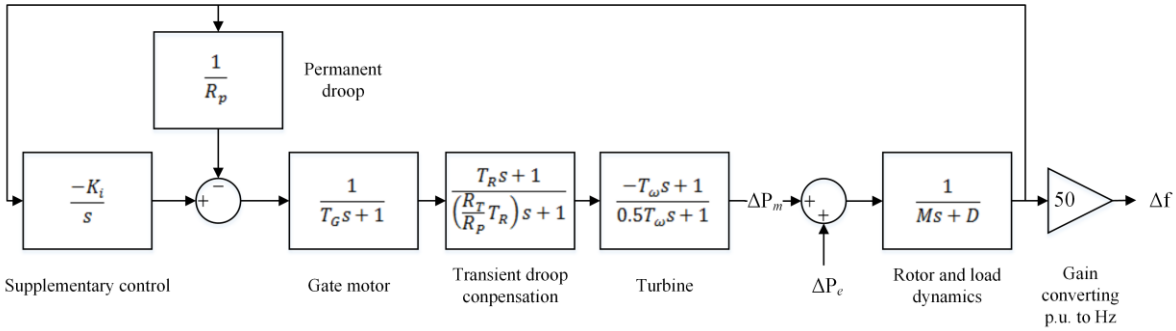

Figure 22: Block diagram illustrating how frequency control is achieved by a typical hydro power plant.

The block diagram in Figure 22 has one input and one output. The input is a power in p.u. representing a change in power drawn from or supplied to the power system. The output is frequency deviation from nominal frequency. The parameters introduced in Figure 22 are summarized and explained in Table 8.

Table 8: Explanation of the parameters introduced in Figure 22 and typical parameter values [29]. *One parameter value, Ki, is taken from* [30].

Prefix	Typical value	Explanation
$\mathbf{R_p}$	0.05	*Permanent droop*. General droop setting (proportional) in the governing control system that makes the change in gate position slower, this to keep frequency stability in the system. A permanent droop is necessary to lower the initial reverse response in power when opening the gate as well as to keep the pressure down in the penstock when the gate closes. A low value results in faster, but more oscillatory, control. This droop setting is used primarily to prevent generating units from working against each other, creating frequency oscillations.
$\mathbf{T_w}$	1.0 s	*Water starting time*. The time it takes for the water to accelerate (from standstill) to a certain velocity (for example maximum velocity physically possible for a certain load). If the gate are to open momentarily with no delay, it will take some time for the water to move in "full speed" in the penstock because of the waters' inertia.
$\mathbf{T_G}$	0.2 s	*Main servo time constant*. Time constant deciding how fast the servo motor controlling the gate will respond to a desired change in gate position. A low value would result in a faster control.
$\mathbf{R_T}$	0.38	*Temporary droop*. Droop setting (proportional) specifically to make the change in gate position slower when there are quick changes in load (disconnection/connection of load or added/disconnected generation). It basically makes the governing control system less sensitive to transients in the system. A high value would result in a slower control system.
M	6.0 s	*Inertia*. Represents the total mechanical inertia in the system. $M = 2 \cdot H$, where H is the inertia constant.
$\mathbf{T_R}$	5.0 s	*Reset time*. Time constant in the transient droop control deciding the time during which the transient droop control should act. A low value would result in a more

		oscillatory but faster control system.
D	1.0	*Load damping constant*. Constant representing the load change due to change in frequency. If D equals one, it means that one percent change in frequency results in one percent change in load.
K_i	3.4	*Supplementary control integrator gain.* Controls the sensitivity of the supplementary control, which purpose is to regulate frequency to the specified nominal value.

7.2 Modeling an islanded power system with hydro- and PV power sources

By combining the hydro model presented in Figure 22 with the PV system model presented in Figure 1, a representation of an islanded power system is constructed. As the hydro model is designed to receive input signals in p.u., the PV panel model is modified to output power in p.u. Also, the DC/DC converter is replaced by an ideal variable voltage controller and the inverter is excluded, this to simplify the PV system. A study is conducted where the frequency quality is analyzed in a case where 10 % of the power comes from the PV system and 90 % of the power comes from the hydro plant. This is represented by scaling the output power from the PV model to be 0.1 p.u. at an irradiance of 1000 W/m^2 (STC). In addition, the inertia (M) in the hydro model is reduced by 10 % to represent an assumed reduction in inertia in the power system due to the lack of inertia in the PV system. The combined hydro- and PV system model is illustrated in Figure 23.

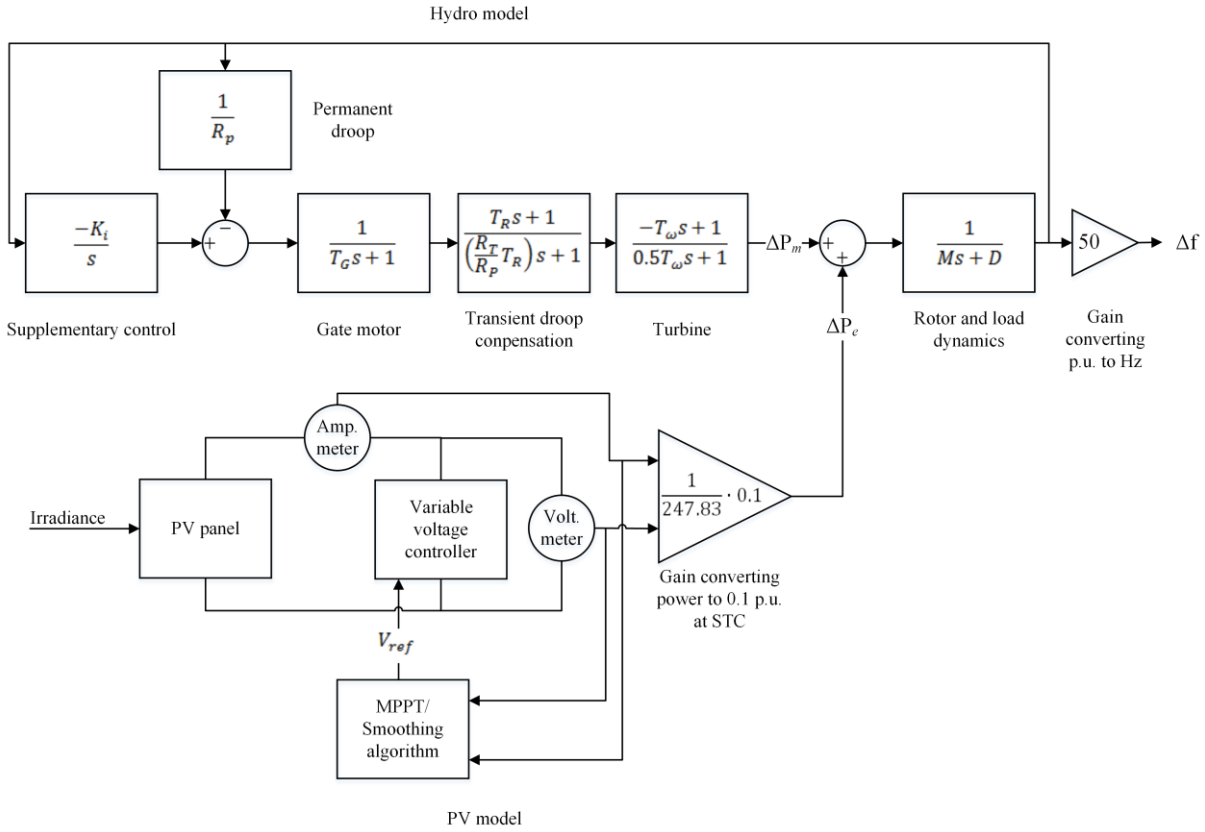

Figure 23: Combined hydro- and PV model.

7.3 Simulation results

7.3.1 Frequency analysis during ramped irradiance input

To compare the frequency behavior with and without the smoothing algorithm, the ramp test irradiance signal from Chapter 5 is used as input to the combined hydro- and PV model. The frequency response for this test signal can be seen in Figure 24. To simplify the analysis of the frequency response, the supplementary control in the hydro model is not used when the test signal is applied (i.e. $K_i = 0$ in the hydro model). This causes the steady state deviation in Figure 24. The power output from the PV model when the ramp test signal is applied, with and without smoothing, is shown in Figure 25.

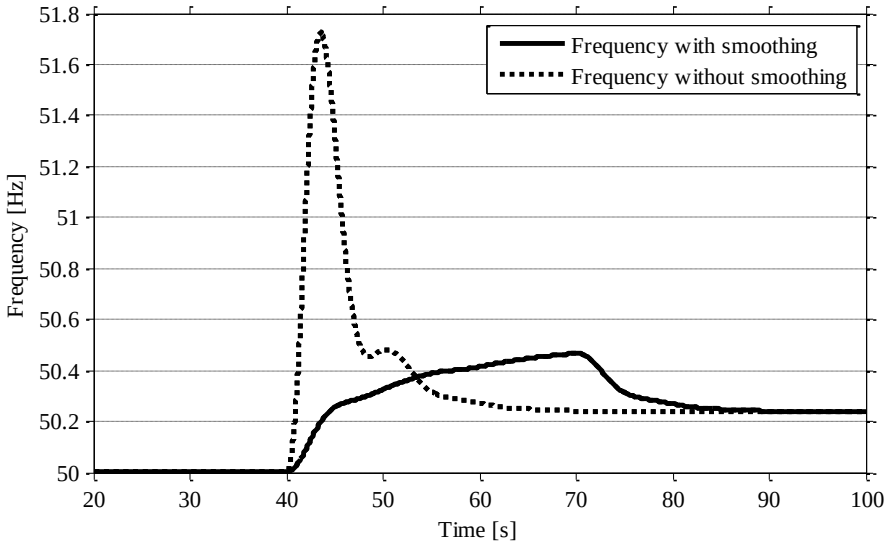

Figure 24: Frequency response from the combined hydro- and PV model when ramp test irradiance signal is applied as input to the PV system. Two cases are presented, one where smoothing is used and one where smoothing is not used.

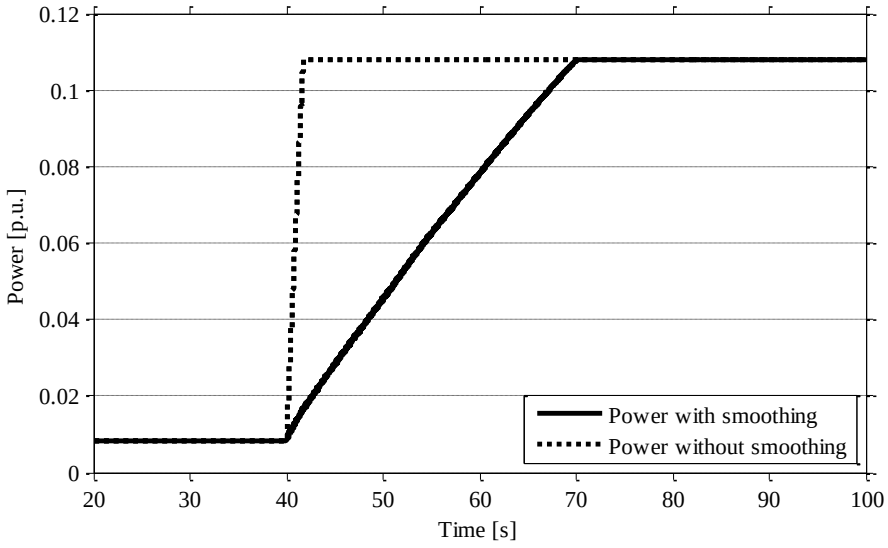

Figure 25: Power output from the PV model when the ramp test irradiance signal is applied. Two cases are presented, one where smoothing is used and one where smoothing is not used.

As can be observed in Figure 24, the frequency deviation is decreased significantly when smoothing is used. The maximum frequency without smoothing is 51.72 Hz and with smoothing it is reduced to 50.47 Hz. The improvement, in terms of reduced frequency deviation, is therefore 73 %. The maximum Rate Of Change Of Frequency, or ROCOF, when smoothing is used is 0.0834 Hz/s. Without smoothing the maximum ROCOF is 0.89 Hz/s. The improvement in terms of reduced ROCOF is therefore 90 %.

7.3.2 Frequency analysis during logged irradiance input

By using the logged irradiance data as input to the combined hydro- and PV model in Figure 23, an evaluation of the frequency quality can be conducted. A case where the smoothing algorithm is used is compared to a case where only the conventional MPPT is used in order to evaluate the frequency quality improvement when using the smoothing algorithm. Irradiance data for all days in April 2015 is used in the simulation. The frequency and PV power within two specific time intervals during the simulation is presented in Figure 26. The first is the interval within which the highest frequency deviation was found, when no smoothing was used, see Figure 26 A and B. The second is the interval within which the highest ROCOF was found, also when no smoothing was used (see Figure 26 C and D).

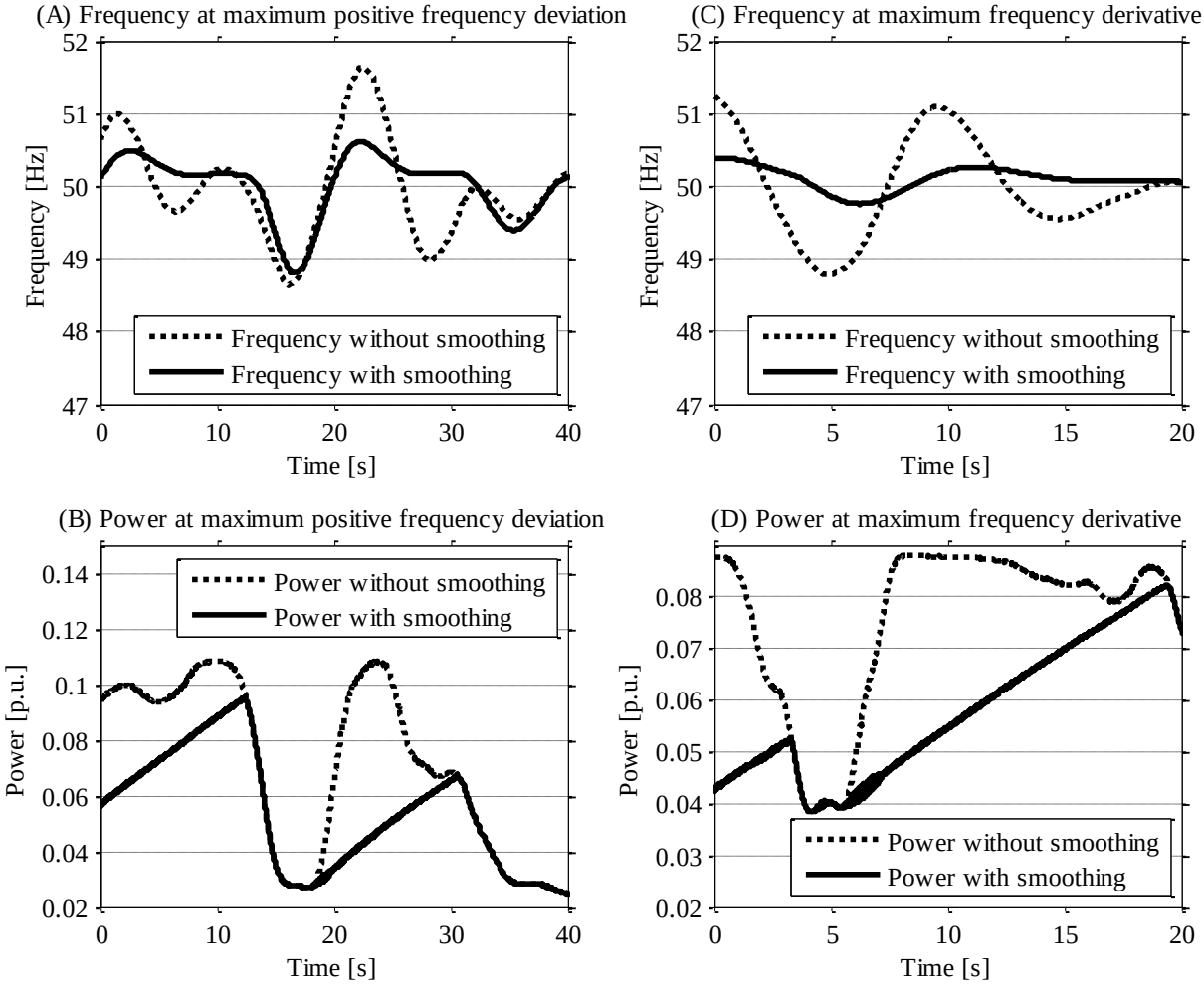

Figure 26: A and B show the frequency and power during 40 seconds around 14.00 on 17 April 2015, which was the time and day in April when the positive frequency deviation was at its maximum when no smoothing was used. C and D show the frequency and power during 20 seconds around 10:40 on 12 April 2015, which was the time and day in April when the frequency derivative was at its maximum when no smoothing was used.

The frequency and power shown in Figure 26 illustrate the effects of power smoothing. By limiting the positive power ramp rate from the PV model, both the maximum positive frequency deviation (see Figure 26 A) as well as the maximum ROCOF (see Figure 26 C) is reduced.

Furthermore, the main results from the simulation of frequency during the month of April are presented in Table 9.

Table 9: Main results from frequency analysis with and without smoothing.

Parameter	Without smoothing	With smoothing	Improvement with smoothing
Max frequency of each day, 30 days mean	50.58 Hz	50.33 Hz	43 % less deviation from 50 Hz
Max frequency in April	51.64 Hz	50.79 Hz	51 % less deviation from 50 Hz
Max ROCOF of each day, 30 days mean	0.30 Hz/s	0.24 Hz/s	20 % reduction
Max ROCOF in April	0.84 Hz/s	0.67 Hz/s	20 % reduction
Time above 50.9 Hz	207 s	0 s	Full improvement
Number of times above 50.9 Hz[1]	261 times	0 times	Full improvement
Energy lost due to smoothing	0 % [2]	0.27 %	No improvement, loss of energy

The results in Table 9 show that for the modeled system, an improvement is accomplished with regards to all parameters presented when smoothing is used, accept for the energy loss. It is expected that energy is lost when smoothing is used, though the loss is relatively small. The most significant improvement can be seen in the maximum frequency, which is reduced significantly when smoothing is used.

Moreover, an analysis was conducted regarding the frequency quality in terms of time duration within certain frequency intervals during the simulation. The result is presented in Table 10.

Table 10: Time (in percentage of the total simulation time) during which the frequency remained within certain intervals when simulating an islanded power system, with and without smoothing, during April 2015.

Frequency interval [Hz]	Without smoothing [%]	With smoothing [%]
$f \geq 50.8$	0.022	0.000
$50.5 \leq f < 50.8$	0.066	0.004
$50.1 \leq f < 50.5$	0.814	0.943
$49.9 \leq f < 50.1$	98.189	98.282
$49.5 \leq f < 49.9$	0.819	0.715
$49.2 \leq f < 49.5$	0.070	0.046
$49.2 < f$	0.019	0.009

From Table 10 it can be concluded that, for the modeled power system, the frequency quality is improved when smoothing is used. In particular the frequency duration above 50.5 Hz is reduced significantly. However, an increased duration between 50.1 and 50.5 can be observed. This is because the time above 50.5 Hz is redistributed over the rest of the intervals when the smoothing is used, the nearest being between 50.1 and 50.5 Hz. Furthermore, the deviation in frequency below 50 Hz is also improved when smoothing is used. This is somewhat unexpected, as the smoothing algorithm is designed to reduce positive frequency deviations. A possible explanation

[1] One time above 50.9 Hz is assumed to last for maximum 1 second. If the frequency remains above 50.9 Hz longer than one second, this is counted as a new "time above 50.9 Hz".
[2] Assuming that conventional MPPT operation is a base case with no loss.

for this is that when irradiance increase and decrease significantly within a short time interval, the reduction in power output will be less significant if smoothing is used, as the reduction in power will happen from a lower initial level. An example of this can be observed in Figure 26 B, where the power output from the PV model decreases rapidly, but from a lower initial value at the time around 12 seconds.

7.4 Further discussion

The simplified power system modeled in this project could represent a power system in island operation with limited regulating capacity. Such configurations exists today and might be a more common scenario in the future, i.e. due to the increased use of energy storage allowing for more independent grid solutions with less system inertia. Moreover, the simplified power system configuration clearly illustrate the effects of power smoothing, even though the simplification has to be taken into consideration when conclusions are made.

It is important to point out that the size of the PV system matters when it comes to the output power characteristics of the system. In a system covering a large area, the ramp rate of the power output will not be as fast as for a small PV system when clouds pass by. This is because it takes time for the cloud to shade/not shade the PV system. This effect is not taken into consideration in this project. Also, in the very common scenario of having PV systems distributed over a large area, a geographical smoothing is expected. This is also not considered in this project. However, the results strongly indicate that frequency improvements can be achieved in certain power system configurations, i.e. if smoothing is used in PV systems connected to a power system with limited inertia and limited regulating capacity.

The smoothing algorithm has not been evaluated when the PV system is shaded none-homogeneously. Such shading might cause the smoothing algorithm not to work properly, especially since it is designed to operate when the MPP is close to the steep negative slope of the IV-curve. When shading is not homogenous, the MPP might move away significantly from the steep negative slope of the IV-curve. In such a case the smoothing algorithm might not work as intended.

The smoothing algorithm parameters chosen in this project might slightly depending on the modeled PV panel. Though, as IV characteristics of PV panels are fairly similar, the dependency will most likely be small, and the algorithm should be considered as a general solution for smoothing power from PV systems. In addition, the methodology used to find the smoothing algorithm parameters can be used for any PV system.

The 0.27 % loss in energy due to smoothing can be put in perspective by comparing with the rate of degradation for PV systems, which is around 0.5 %/year [31], thus the energy loss can be considered relatively small. Though, 0.27 % might anyway constitute a problem in economic terms, depending on the economic margin of the PV system investment.

A solution to simplify a possible introduction of smoothing functionality in conventional inverters may be to offer an additional economic compensation for using a PV system with power smoothing. In Sweden today, PV system owners receive an economic compensation for feeding power to the grid [32]. The rate depends on how much support the PV system is considered to offer the grid owner in terms of stability and loss reduction. An additional economic compensation for using smoothing functionality might be an alternative in the future.

8 Conclusions and future work

8.1 Conclusions

In this project, a power smoothing algorithm has been developed and implemented in a modeled PV system. The PV system is connected to a simplified power system model and an analysis of the frequency quality with and without smoothing is conducted. The analysis shows that the smoothing algorithm improves the frequency quality in the simplified power system model. The mean- and maximum positive frequency deviation improves by approximately 40 % and 50 % respectively. Furthermore, the maximum ROCOF and mean ROCOF are both reduced by 20 %. The time at which the frequency remains above 50.9 Hz reduces from 207 seconds to zero seconds. The time at which the frequency is above 50.5 Hz reduces from 8.8 % to 0.4 % and the time at which the frequency is below 49.5 Hz reduces from 8.9 % to 5.5 %. The energy lost due to power smoothing is 0.27 %. This can be compared to the average degradation of PV systems, which is around 0.5 % per year [31].

Furthermore, a PV panel has been characterized and used as a base for developing a PV panel model. Staring from the one diode model of a PV cell, a method to determine the model parameters of a PV panel is further developed. To determine how well the further developed model fits the measured values of the characterized PV panel, an error analysis using RSS is used. The RSS sums the difference between each data point of two curves, and the result is the total sum of errors. When the IV characteristics of the further developed model are compared to the measured IV characteristics of the PV panel, the RSS error between them is 1.30. When the European standard is used to find one of the model parameters, R_s, and the rest of the model parameters are iterated to find the best fit to the measured values, the smallest RSS error between the modeled and the measured IV-curves is found to be 3.17. Thus, the method further developed in this project proves to give the smallest RSS error. However, RSS is one of many ways to determine how well one curve fits to another. Nevertheless, the fact that the further developed method gives a good fit to the measured values indicates that it is a valid method for use in the characterization of PV panel parameters.

8.2 Future work

There are several parts of the project that can be developed and analyzed further. The smoothing algorithm can be modified to save the power value a few seconds before the present power value to detect fast and short dips in power. By making sure that the smoothing algorithm is not activated during fast and short dips in power, the frequency might become more stable due to the system inertia. In addition, power smoothing could be combined with batteries or capacitors, which can temporarily store and supply energy, this to reduce losses.

A possible way to further improve the frequency quality using power smoothing could be to test different maximum ramp rates during smoothing. One way to find appropriate ramp rates might be to iteratively change the ramp rate, keeping the same irradiance input sequence at each iteration. The frequency quality at different ramp rates can then be compared and a best case can be identified. The irradiance data could either be actual irradiance data or an irradiance sequence that represent typical irradiance variations. In addition, it might be possible to find a relation between the size of a PV system and the ramp rate limitation giving the best frequency improvement.

Furthermore, smoothing could be done when irradiance decreases rapidly. This can be achieved using energy storage, but it might also be possible to achieve a slight power smoothing effect by predicting upcoming negative irradiance changes through statistical analysis, i.e. a fast irradiance decrease might statistically be preceded by certain irradiance characteristics. If such predictions are possible, the smoothing algorithm developed in this project could be modified to limit negative power ramp rates without any fundamental changes in the algorithm. Moreover, a thorough analysis regarding the cause of the reduced time duration for under-frequencies when using the smoothing algorithm could be conducted.

Additionally, an analysis could be conducted where many PV systems are simulated with a certain geographical distance from each other. Such analysis might further clarify if power smoothing improves frequency quality, as it would represent a more realistic case. Lastly, analysis regarding the effects of power smoothing on voltage stability could be conducted.

References

[1] Entsoe, "Introduction in Automatic FRR," 2012.

[2] J. P. Lopes, "Integrating distributed generation into electric power systems: A review of drivers, challenges and opportunities," *Electric Power Systems Research,* p. 1189–1203, July 2007.

[3] G. Corbetta, "Wind in power 2014 European statistics," THE EUROPEAN WIND ENERGY ASSOCIATION, Giorgio Corbetta, 2015.

[4] J. Lindahl, "Svensk sammanfattning av IEA-PVPS National Survey Report of PV power applications in Sweden 2014," International Energy Agency Photovoltaic Power System Programme, Swedish Energy Agency, Uppsala, 2015.

[5] K. B. P. Z. e. Jens. C. Boemer, "Overview of German Grid Issues and Retrofit of Photovoltaic Power Plants in Germany for the Prevention of Frequency Stability Problems in Abnormal System Conditions of the ENTSO-E Region Continental Europe," in *1st International Workshop on Integration of Solar Power into Power Systems,* Aarhus, 2011.

[6] I. de la Parra, "Management of PV Power Generation - Less variability and more predictability," in *PV Crops Parralel Event at 29th PVSEC,* Amsterdam, 2014.

[7] S. Kumar, "India to build world's largest solar plant," Nature International weekly jurnal of science, 4 2 2014. [Online]. Available: http://www.nature.com/news/india-to-build-world-s-largest-solar-plant-1.14647. [Accessed 07 07 2015].

[8] E. Meza, "pv-magazine.com," 17 03 2015. [Online]. Available: http://www.pv-magazine.com/news/details/beitrag/italy-to-switch-off-pv-plants-over-100-kw-during-solar-eclipse_100018639/#axzz3fZf2NQYi. [Accessed 11 07 2015].

[9] FRAUNHOFER ISE, "Photovoltaics Report Freiburg," FRAUNHOFER INSTITUTE FOR SOLAR ENERGY SYSTEMS ISE, Freiburg, 2014.

[10] T. a. C. P. Esram, "Comparison of Photovoltaic Array Maximum Power Point Tracking Techniques," *Energy Conversion, IEEE Transactions on,* vol. 22, no. 2, pp. 439-449, 2007.

[11] National Instruments, "Code for downloads USB-6009," 03 06 2009. [Online]. Available: http://www.ni.com/example/31213/en/. [Accessed 02 04 2015].

[12] Entsoe, "entsoe.eu," 15 1 2007. [Online]. Available: https://www.entsoe.eu/fileadmin/user_upload/_library/publications/nordic/planning/070115_entsoe_nordic_NordicGridCode.pdf. [Accessed 07 07 2015].

[13] W. S. Cleveland, "Robust Locally Weighted Regression and Smoothing Scatterplots," *Journal of the American Statistical Association,* vol. 74, no. 368, pp. 829-836, 1979.

[14] J. Burkey, "LOWESS, Locally Weighted Scatterplot Smoothing for linear and non-linear data (enhanced)," MathWorks, 18 06 2012. [Online]. Available: http://www.mathworks.com/matlabcentral/fileexchange/22470-lowess--locally-weighted-scatterplot-smoothing-for-linear-and-non-linear-data--enhanced-/content//lowess.m. [Accessed 01 04 2015].

[15] J. R. G. E. R. F. Marcelo Gradella Villalva, "MODELING AND CIRCUIT-BASED SIMULATION OF PHOTOVOLTAIC ARRAYS," in *Power Electronics Conference*, Brazilian, 2009.

[16] J. A. S. A. C. Carrero, "A single procedure for helping PV designers to select silicon PV modules and evaluate the loss resistances," *Renewable Energy,* vol. 32, no. 15, p. 2579–2589, 2007.

[17] Math Works, "Solar Cell," [Online]. Available: http://se.mathworks.com/help/physmod/elec/ref/solarcell.html. [Accessed 02 04 2015].

[18] M. D. Archer and R. Hill, Clean Energy From Photovoltaics, London: Imperial Collage Press, 2001.

[19] K. Jeppson, Kurshäfte i Microelectronik, Gothenburg: Chalmers Tekniska Högskola, Institutionen för mikroteknologi och nanovetenskap, 2011.

[20] S. S. Luis Castaner, MODELLING PHOTOVOLTAIC SYSTEMS Using Pspice, Chichester: John Wiley & Sons, LTD, 2002.

[21] Agilent Technologies, "ccontrols.ch," 04 11 2009. [Online]. Available: http://www.ccontrols.ch/cms/upload/applikationen/Solar-Cell/5990-4428EN.pdf. [Accessed 02 04 2015].

[22] S. B. Christiana Honsberg, "Shunt Resistance," PVEDUCATION.ORG, [Online]. Available: http://www.pveducation.org/pvcdrom/solar-cell-operation/shunt-resistance. [Accessed 02 04 2015].

[23] I. Mathiasson, *EEK231 Laboratory exercise Solar energy and solar cells,* Gothenburg: Chalmers Univerity of Technology, Department of Energy and Environment, Division of Electric Power Engineering, 2009.

[24] MathWorks, "Accelerating the pace of engineering and science," [Online]. Available: http://se.mathworks.com. [Accessed 02 04 2015].

[25] H. Smith, Applied regression analysis, New York: Wiley, 1998.

[26] N. H. H. H. R. Bründlinger, "prEN 50530 - The new european standard for performance characterisation of PV inverters," in *European Photovoltaic Solar Energy Conference and Exhibition (EU PVSEC)*, Hamburg, 2009.

[27] SMA, "sma-america.com," 2014. [Online]. Available: http://files.sma.de/dl/21561/STPTL-US12-24-DUS143110W.PDF. [Accessed 08 07 2015].

[28] Svenska Kraftnät, "Storskalig utbyggnad av vindkraft Konsekvenes för stamnätet och behovet av reglerkraft," 2008.

[29] P. Kundur, Power system stability and control, New York: McGraw-Hill, 1994.

[30] M. Persson, "Frequency Response by Wind Farms in Islanded Power Systems with High Wind Power Penetration," Chalmers University of Technology, Gothenburg, 2015.

[31] S. R. K. Dirk C. Jordan, "Photovoltaic Degradation Rates — An Analytical Review," NREL, Springfield, 2012.

[32] E.ON Elnät, "eon.se," 2014. [Online]. Available: https://www.eon.se/upload/dokument/Eln%c3%a4t/Prislista_Elmikroproduktion_Syd_Sthlm_140101.pdf. [Accessed 10 07 2015].

[33] D. Mencke, *e-mail correspondence,* 2014.

Appendix I

Data sheets for the irradiance sensor SiS-13TC-T:

SILICON IRRADIANCE SENSOR

Technical Data

SI-SENSOR
General information

- Solar cell: Monocrystalline Silicon (20 mm x 34 mm)
- Current shunt: 0,27 Ω (TC = 20 ppm / K)
- Operating temperature: –20 °C to 70 °C
- Electrical connection done via shielded cable, length 3 m
- Case, protection mode: Powder-coated aluminum, IP 67
- Dimension, weight: 138mm x 64mm x 40mm, appr. 440 g

ACCURACY
Irradiance

- Error with temperature compensation compared to pyranometer within the operating range of -20 °C to 70 °C and vertically beam of irradiance: ± 5 % at 1000 W/m²
- Non-linearity of the electronic circuit:± 0,3% from reading for 50 to 1300 W/m²

Temperature

- Accuracy at 25 °C: ± 1,5 °C
- Non-linearity: ± 0,5 °C
- Error (over operating temperature range of -20…-70°C): ± 2,0 °C

Customs Numbers

for all silicon irradiance sensors: 85 41 40 90

Sensor Types:

Typ	Irradiance			Cell Temperature
	Power Supply	Temperature Compensation	Output Signal	Output Signal
SiS-01TC	5 to 28 V_{DC}	Yes	0 to 1 V per 0 to 1000 W/m²	./.
SiS-01TC-T	5 to 28 V_{DC}	Yes	0 to 1 V per 0 to 1000 W/m²	1,235 V + T[°C]*10mV/°C
SiS-02	./.	No	appr. 60 mV per 1000 W/m²	./.
SiS-02-Pt100 SiS-02-Pt1000	./.	No	appr. 60 mV per 1000 W/m²	Pt100, class A Pt1000, class A
SiS-420TC	12 to 28 V_{DC}	Yes	4 to 20 mA per 0 to 1200 W/m²	./.
SiS-420TC-T	12 to 28 V_{DC}	Yes	4 to 20 mA per 0 to 1200 W/m²	(13,88+0,08/°C*T[°C])mA
SiS-13TC	12 to 28 V_{DC}	Yes	0 to 10 V per 0 to 1300 W/m²	./.
SiS-13TC-T	12 to 28 V_{DC}	Yes	0 to 10 V 0 to 1300 W/m²	2,268V+86,9mV/°C*T

Measurement Error Si- / SiS- Sensors

	Condition	Typ (use Si- values also for SiS- types)	Error (% of range)
Response Time (99%)		Si-02	0.001 s
	>50W/m²	Si-01 / -13 / -420	0.15 s
		Si-RS485 / -CANopen	1 s
Offset		Si-02	0.01%
		Si-01 / -13	typ. <0.25% / max. 0.65%
		Si-420	typ. < 0.25% / max. 0.9%
		Si-RS485 / -CANopen	typ. < 0.15%/ max. 0.6%
Stability p.a.		all	typ. 0.5%
Non-linearity of Electrical Circuit		Si-02	0.01%
		Si-01 / -13 / -420 / -RS485 / -CANopen	0.1%
Incident Angle Modifier	45°	all	typ. 2%
Temperature Error	-20..+70°C	Si-02 (with ext. compensation)	typ. 0.2 / max. 0.35%
	-20..+70°C	Si-02 (without ext. compensation)	max. 2.5%
	-20..+70°C	Si-01 / -13 / -420	typ. 0.4% / max. 0.9%
	-20..+70°C	Si-RS485 / -CANopen	typ. 0.4% / max. 0.8%
Inhouse Calibration			
Repeatability of Calibration to Reference		all	1,0%
Max. Error of Reference at STC / vertically light beam		all	2,0%
Default Calibration ISE			
Max. Error at STC / vertically light beam		all	2.5%
Precision Calibration ISE			
Max. Error at STC / vertically light beam		all	2,0%

Data sheet for the amplifier/voltage follower AD620ND:

ANALOG DEVICES

Low Cost, Low Power Instrumentation Amplifier

AD620

FEATURES
EASY TO USE
Gain Set with One External Resistor
(Gain Range 1 to 1000)
Wide Power Supply Range (±2.3 V to ±18 V)
Higher Performance than Three Op Amp IA Designs
Available in 8-Lead DIP and SOIC Packaging
Low Power, 1.3 mA max Supply Current

EXCELLENT DC PERFORMANCE ("B GRADE")
50 μV max, Input Offset Voltage
0.6 μV/°C max, Input Offset Drift
1.0 nA max, Input Bias Current
100 dB min Common-Mode Rejection Ratio (G = 10)

LOW NOISE
9 nV/√Hz, @ 1 kHz, Input Voltage Noise
0.28 μV p-p Noise (0.1 Hz to 10 Hz)

EXCELLENT AC SPECIFICATIONS
120 kHz Bandwidth (G = 100)
15 μs Settling Time to 0.01%

APPLICATIONS
Weigh Scales
ECG and Medical Instrumentation
Transducer Interface
Data Acquisition Systems
Industrial Process Controls
Battery Powered and Portable Equipment

PRODUCT DESCRIPTION
The AD620 is a low cost, high accuracy instrumentation amplifier that requires only one external resistor to set gains of 1 to

CONNECTION DIAGRAM

8-Lead Plastic Mini-DIP (N), Cerdip (Q) and SOIC (R) Packages

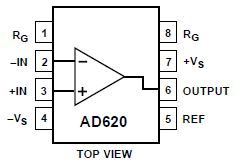

TOP VIEW

1000. Furthermore, the AD620 features 8-lead SOIC and DIP packaging that is smaller than discrete designs, and offers lower power (only 1.3 mA max supply current), making it a good fit for battery powered, portable (or remote) applications.

The AD620, with its high accuracy of 40 ppm maximum nonlinearity, low offset voltage of 50 μV max and offset drift of 0.6 μV/°C max, is ideal for use in precision data acquisition systems, such as weigh scales and transducer interfaces. Furthermore, the low noise, low input bias current, and low power of the AD620 make it well suited for medical applications such as ECG and noninvasive blood pressure monitors.

The low input bias current of 1.0 nA max is made possible with the use of Superβeta processing in the input stage. The AD620 works well as a preamplifier due to its low input voltage noise of 9 nV/√Hz at 1 kHz, 0.28 μV p-p in the 0.1 Hz to 10 Hz band, 0.1 pA/√Hz input current noise. Also, the AD620 is well suited for multiplexed applications with its settling time of 15 μs to 0.01% and its cost is low enough to enable designs with one in-amp per channel.

Data sheets for the logger NI-USB-6009:

Technical Sales
Sverige
08 587 895 00
ni.sweden@ni.com

NI USB-6009

14-Bit, 48 kS/s Low-Cost Multifunction DAQ

- 8 analog inputs (14-bit, 48 kS/s)
- 2 static analog outputs (12-bit); 12 digital I/O; 32-bit counter
- Bus-powered for high mobility; built-in signal connectivity
- OEM version available
- Compatible with LabVIEW, LabWindows™/CVI, and Measurement Studio for Visual Studio .NET

Analog Input	
Single-Ended Channels	8
Differential Channels	4
Analog Input Resolution	14 bits
Maximum Voltage Range	
Range	-10 V - 10 V
Accuracy	7.73 mV
Minimum Voltage Range	
Range	-1 V - 1 V
Accuracy	1.53 mV
Number of Ranges	8
Simultaneous Sampling	No
On-Board Memory	512 B

Appendix II

Commented photos of equipment built or used during the project:

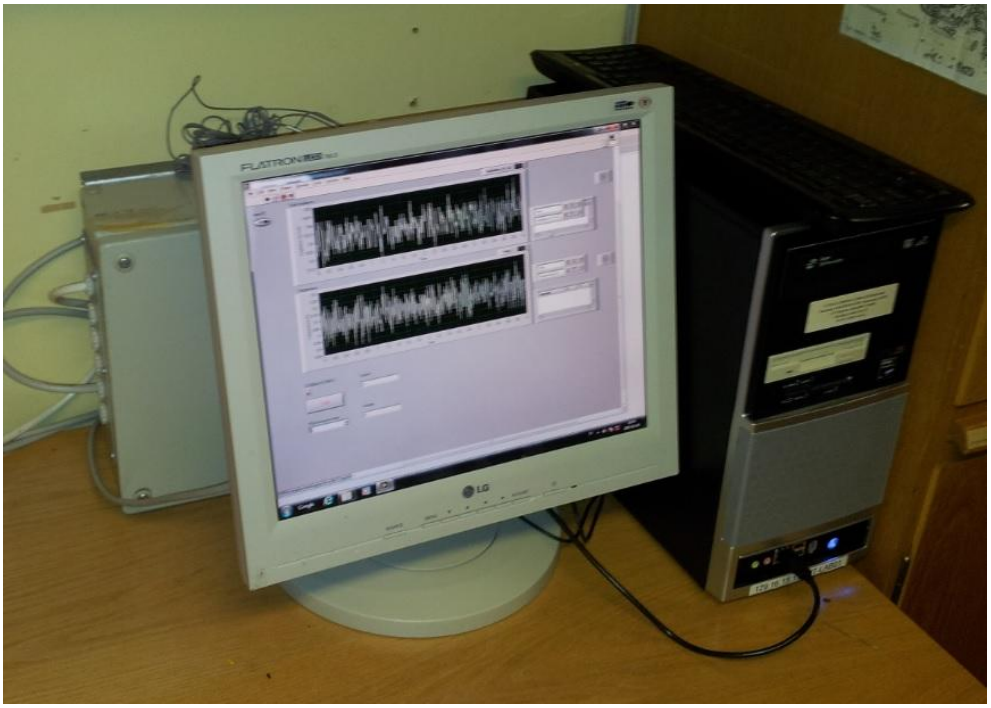

Figure 27: Logging arrangement at Chalmers research facility on the island of Hönö, near Gothenburg. The picture shows the computer running the LabView software, which processes and saves the irradiance data.

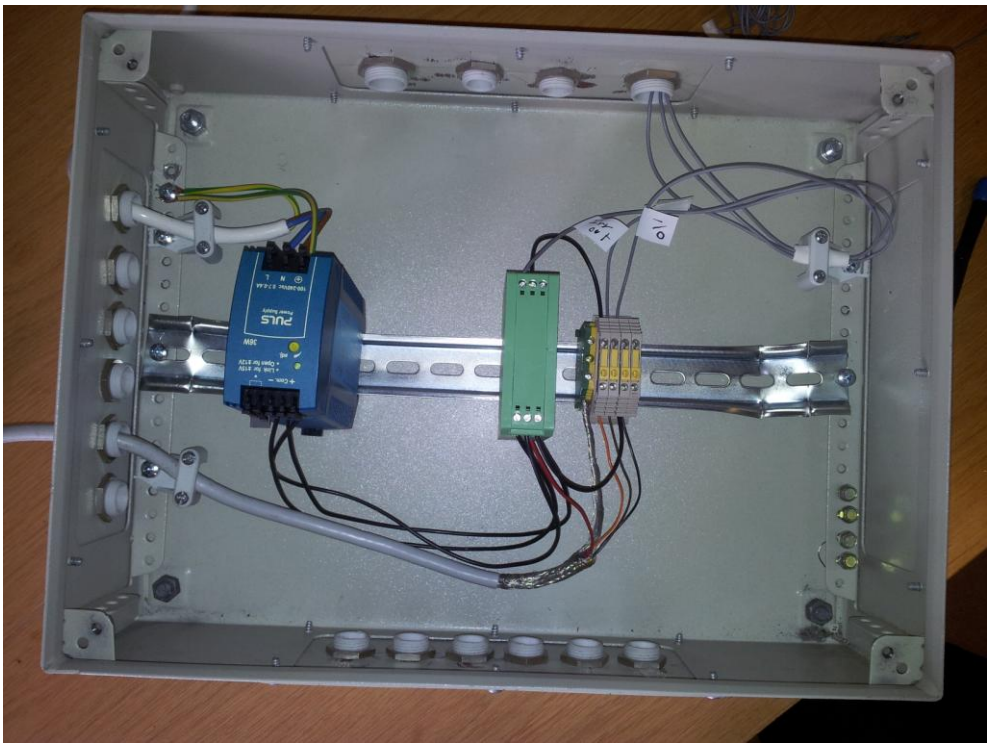

Figure 28: Encapsulating metallic box used for protection of parts of the logging equipment. From the left: AC-DC power supply, voltage follower circuit and connection blocks. The voltage follower circuit is encapsulated in the green plastic casing for protection and to make it mountable in the metallic box.

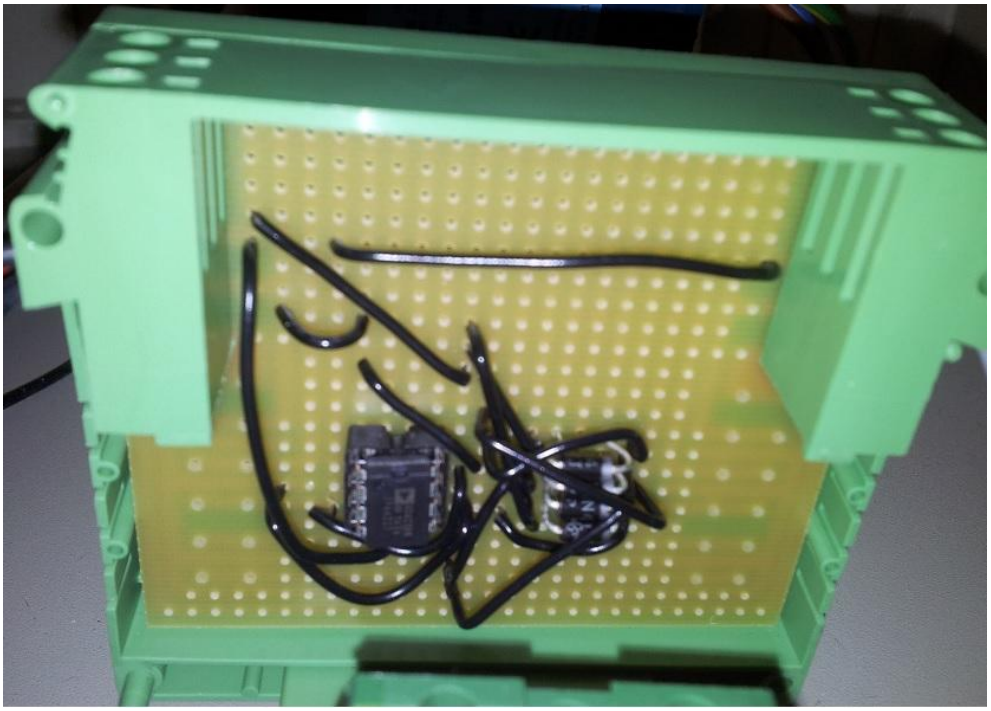

Figure 29: Voltage follower circuit implemented on a circuit board. The photo shows the AD620AN circuit, the protective diodes and the ancillary wiring.

Appendix III

Additional figures with comments

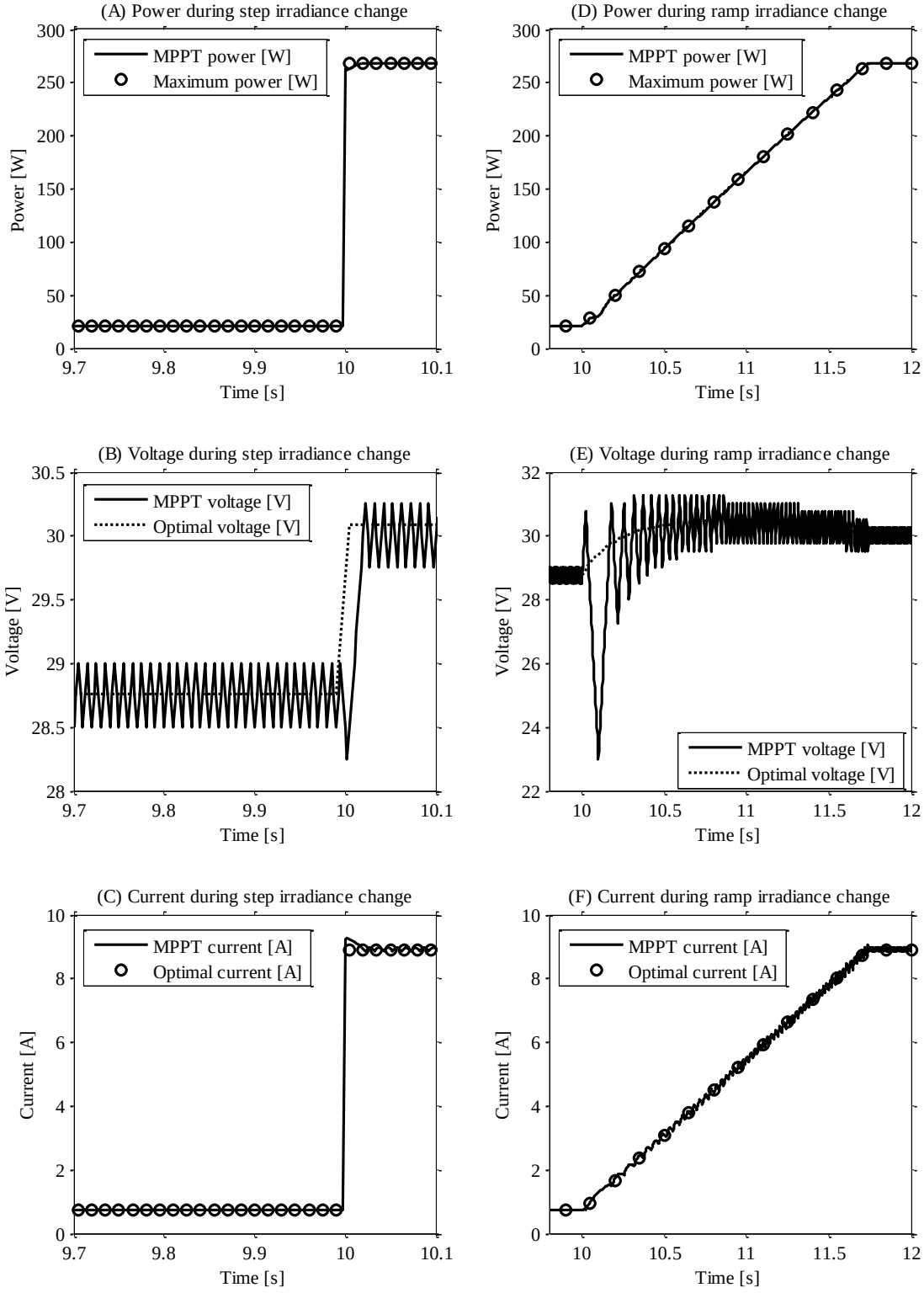

Figure 30: Voltage and current output from the MPPT when irradiance test signals are applied to the modeled PV panel. Also, the maximum power and optimal voltage and current (from Figure 18) are presented, this to illustrate the difference between the MPPT output and the optimal values. In A, B and C, the power, voltage and current during an applied step irradiance test signal are illustrated. The same entities are presented in D, E, and

F, but for an applied ramp irradiance test signal. It can be concluded that the MPPT works satisfactory when step and ramp test irradiance signals are applied.

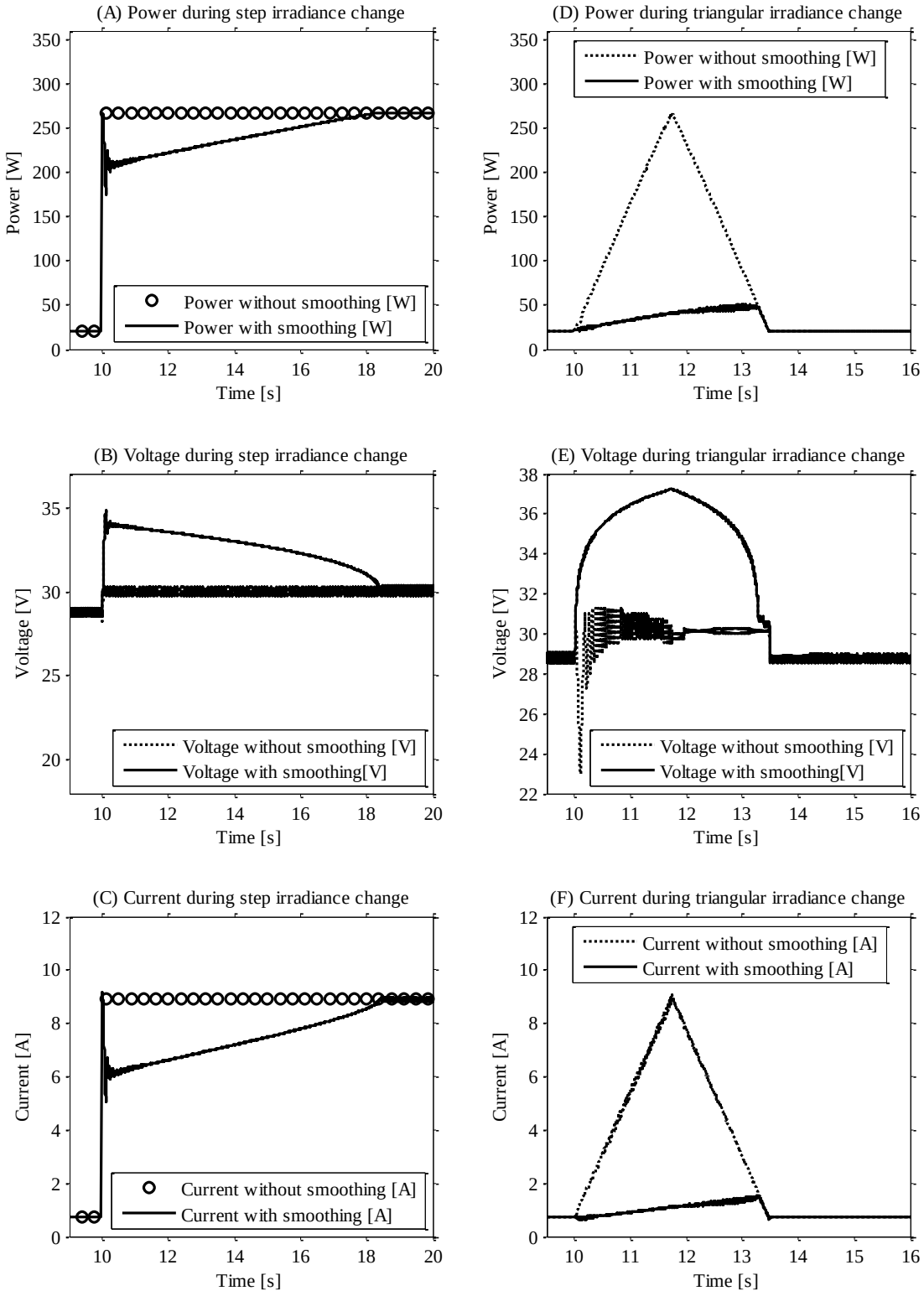

Figure 31: Power, voltage and current output from PV model with and without smoothing when step- and triangular test signals are applied.

In Figure 31 A, it can be observed that when a step change in irradiance is applied, the smoothing algorithm is not able to smooth the power as intended. As can be observed in Figure 31 B, the voltage is increased rapidly just after the irradiance step is applied, though this is not fast enough

to achieve the power limitation needed to smooth the power output at the intended maximum ramp rate. Instead there is an initial rapid power increase both with and without smoothing. In the case when smoothing is used, the power is somewhat reduced after the initial increase, than the power is ramped with a ramp rate of around 7.4 W/s. The purpose of Figure 31 A, B and C is to illustrate that if the irradiance increase faster than what the smoothing algorithm is designed for, the smoothing functionality will not work as intended. Though, a step change in irradiance will not be found in real irradiance data. The result from applying a triangular test signal is illustrated in Figure 31 C, D and E. The ramp rate during the smoothing sequence is around 9.7 W/s, which is slightly higher than the intended. Nevertheless, it can be concluded that a triangular test signal can be smoothed without any significant deviation from the intended smoothing ramp rate.

Short elaboration on MPPT implementation using PI controller

The IncCond method can be implemented using a proportional integral (PI) control [10]. This implementation is not used in this project, but as future work might include implementing IncCond using PI control, this technique will be described briefly. A PI controller can be used to drive an error signal to zero. From [10] it is known that an error signal, denoted e, can be defined using (19) according to

$$\frac{(dP/dV)}{V} - \frac{I}{V} = \frac{\Delta I}{\Delta V} \Rightarrow \left\{\frac{(dP/dV)}{V} = e\right\} \Rightarrow e - \frac{I}{V} = \frac{\Delta I}{\Delta V} \Rightarrow e = \frac{I}{V} + \frac{\Delta I}{\Delta V} \qquad (24)$$

As can be observed in (24) the incremental conductance and instantaneous conductance can be used to generate an error signal. From (20) we know that if $dP/dV \neq 0$, operation is not at the MPP. A deviation from the operation at the MPP can be seen as the error, e. By combining (20) and (24), it can be concluded that the error will be positive if operation is on the left side of MPP on the PV-curve. The PI controller should then output an increased voltage reference. If operation is on the right side of MPP, the error will be negative and the PI controller should output a decreased voltage reference. In this way a PI controller can track the MPP.

Appendix IV

Verification of logging setup functionality

To verify the logging setup functionality, tests were performed on the voltage follower and sensor. Important properties for the voltage follower are to not affect the amplitude of the voltage signal or have a slower response time than the sensor. For the sensor it is important with a fast response time, this to be able to log fast irradiance changes.

Voltage follower tests

A test was performed to evaluate the voltage follower's impact on a constant voltage signal. A series of test voltages were supplied to the input of the voltage follower and measurements were taken both at the input and output using an oscilloscope. The output voltage was also measured with the logger. The results are presented in Table 11.

Table 11: Test voltages measured at the input and output of the voltage follower (AD620AN). The output voltage was measured both with oscilloscope and with the logger (NI-USB-6009). A 10 V signal corresponds to an irradiance of 1300 W/m^2, see irradiance sensor datasheet in Appendix I.

Voltage follower input [V]	Voltage follower output [V]	Logger [V]
9.59	9.57	9.58
7.97	7.93	7.96
3.42	3.38	3.42
1.10	1.07	1.08
0.358	0.347	0.348
0.125	0.120	0.124
0	0.003	0.004

From Table 11 it can be concluded that there is no significant change in voltage due to the use of the voltage follower. Moreover, it can be concluded that voltages below 0.484 V can be detected and measured by the logger when the voltage follower is used.

Furthermore, a test was performed to make sure the voltage follower did not affect the response time of the irradiance sensor. This is important, as one of the main purposes of the irradiance logging is to analyze the rate of change in irradiance. A signal generator was used to generate a voltage signal ramping form 0 to around 10 V at the voltage follower input. This voltage level was chosen as the voltage range of the irradiance sensor and logger is 10 V. The result from the test can be seen in Figure 32.

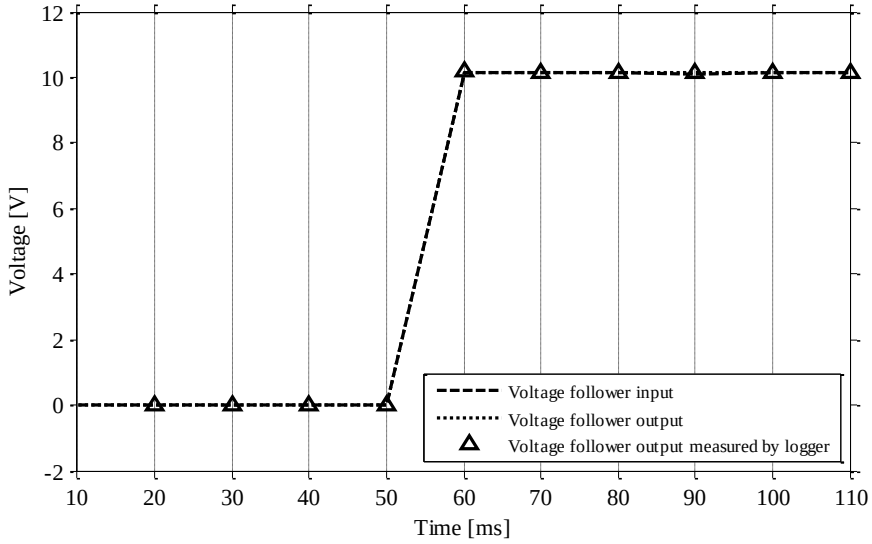

Figure 32: Rise time test when applying a 10.16 V square wave voltage pulse.

From Figure 32 it can be concluded that the voltage follower does not affect the response time of the irradiance sensor in a way that is significant for this project. The signal generator was also used to test the fall time and it was concluded that both the rise- and fall times were below 10 ms.

Irradiance sensor test

To ensure that fast changes in irradiance are captured accurately, the response time of the irradiance sensor was evaluated. In order to do this, a halogen lamp was used, which was placed at different distances from the irradiance sensor to simulate different levels of irradiance. By switching the lamp on and off, pulses of irradiance was sent to the irradiance sensor. The result from the test, logged by the NI-USB-6009 logger, is presented in Figure 33.

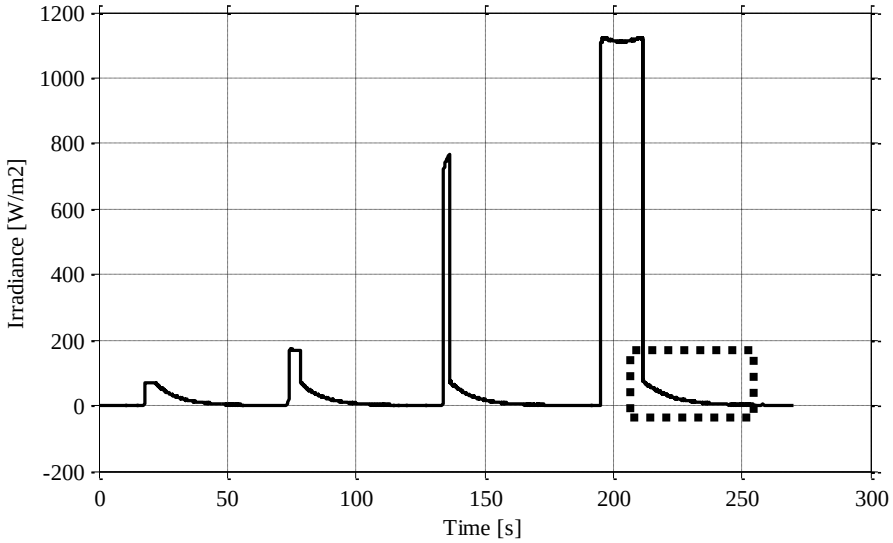

Figure 33: Response time test for irradiance sensor SiS-13TC-T.

As can be observed in Figure 33, the irradiance sensor was subjected to four light pulses from the lamp, each with different magnitude (corresponding to different distances between the lamp and the sensor). The small variations that can be observed when the sensor is irradiated (at the maximum values of the pulses) are due to oscillations in the light from the lamp. In Table 12, the resulting response times are presented for the different pulses. One fast and one slow negative response time are presented. This is because the rate of change during voltage decrease is reduced significantly at around 0.65 V (corresponding to 85 W/m^2). The reduced rate of change can be observed in the dashed rectangular box in Figure 33. A hypothesis to why this occurs is that a built-in capacitor at the output of the sensor (100 µF [33]) delay the voltage decrease, this because it takes time for capacitor to discharge. This delayed voltage decrease does not constitute any significant problem in this project, as the rate of change in irradiance below 85 W/m^2 is not very important for the frequency quality analysis.

Table 12: Response times for the irradiance pulses in Figure 33.

Pulse magnitude	**0.5 V**	**1.3 V**	**5.8 V**	**8.6 V**
Positive response time [s]	0.24	0.27	0.27	0.23
Negative response time (fast) [s]	-	0.06	0.18	0.2
Negative response time (slow) [s]	31.8	32.3	34.5	39.9

From Table 12 it can be concluded that voltage pulses with higher magnitude lead to longer negative response times. The positive response times differ to some extent depending on pulse magnitude, but there is no correlation between pulse magnitude and positive response time. Furthermore, the response time of the sensor could be affected by the characteristics of the lamp used in the test. It may take time for the lamp to reach full illumination, as well as to go from illuminated to complete darkness. These two times can also be different. This could partly explain why the positive and fast negative response times is in the range of 200 to 300 ms and 60 to 200 ms respectively. According to the data sheet of the sensor (see Appendix I), the response time for reaching 99 % of the actual irradiance is 150 ms if the irradiance is constantly above 50 W/m^2 (corresponding to approximately 0.39 V). In the test the initial irradiance is around 0 W/m^2, which partly could explain why the positive response time is longer than that stated in the data sheet. The fast negative response time is approximately the same as that stated in the datasheet, the longest being 200 ms for the pulse with the highest magnitude.

Short elaboration on an error in the logged irradiance data

In Figure 5 in section 3.4 the steepest irradiance derivatives each day in April are illustrated, where the steepest is found on 29 of April, -1856 W/m^2/s. The irradiance at the time when this derivative occurs can be seen in Figure 34.

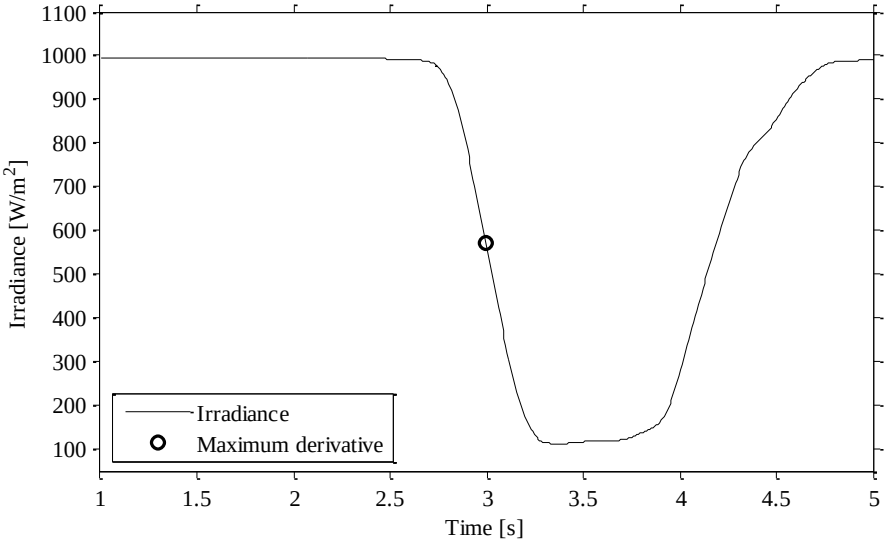

Figure 34: Irradiance change and maximum derivative during 5 seconds on 29 of April around 15.00, when the steepest derivative from Figure 5 occurs.

The derivative occurs when the irradiance rapidly changes from around 1000 W/m^2 to around 100 W/m^2 and then back to 1000 W/m^2 again, and the dip lasts for approximately 1.5 seconds, which is very short. This in combination with the fact the derivative is significantly steeper than the steepest derivatives the other days of the month, indicates that the dip is a result of an object passing relatively close to the sensor, shading it temporarily. Such object could for example be a bird or a leaf. The dip could also be a result of an unknown measurement error.

Appendix V

Matlab codes:

```
%%Create parameters for PV panel model-------------------------------------

Rs = 0.36;                    %Equivalent series resistance.
Rp = 235;                     %Equivalent parallel resistance.
Isc_measured = 8.81521;       %Short circuit current.
Voc_measured = 37.7285;       %Open circuit voltage.
Isc = Isc_measured + ((Isc_measured*Rs)/Rp); %Short circuit current if
                              %Rs and Rp are changed to 0 and infinite
                              %respectively.
Voc = Voc_measured;           %Open circuit voltage if Rs and Rp are changed
                              %to 0 and infinite respectively (no change).
I_at_mpp_measured = 8.23432; %Measured current at the MPP.
V_at_mpp_measured = 30.0973; %Measured voltage at the MPP.
V_at_mpp = V_at_mpp_measured + (Rs*I_at_mpp_measured); %Voltage at MPP if
                              %Rs and Rp are changed to 0 and infinite
                              %respectively.
I_at_mpp = I_at_mpp_measured + ((V_at_mpp+(I_at_mpp_measured*Rs))/Rp);
                              %Current at MPP if Rs and Rp are changed to 0
                              %and infinite respectively.
T_measured = 25;              %Temperature at STC.
T_kelvin = T_measured + 273.15; %Convert Celsius to Kelvin.
Idiod1 = Isc;                 %Diode current at open circuit if Rs and Rp
                              %are changed to 0 and infinite respectively.
Idiod2 = Isc - I_at_mpp;      %Diode current at MPP
Udiod1 = Voc;                 %Diode voltage at open circuit if Rs and Rp
                              %are changed to 0 and infinite respectively.
Udiod2 = V_at_mpp;            %Diode voltage at MPP if Rs and Rp are
                              %changed to 0 and infinite respectively.

C_diod = (log(Idiod2)-log(Idiod1))/(Udiod2-Udiod1); %Help variable to
                              %simplify further expressions.
I_0 = Idiod1/exp(C_diod*Udiod1); %Diode reverse bias saturation current
n = 1/(C_diod*(8.62*10^-5)*T_kelvin); %Diode ideality factor for PV panel.
n_per_cell = n/60;            %Diode ideality factor for one cell (60 cells
                              %in the PV panel).

%%END Create parameters for PV panel model---------------------------------

%%Create parameters for smoothing algorithm--------------------------------

power_slope_allowed = 8.227;     %Maximum ramp rate (W/s)
delta_power_vector_length = 60; %Nr. of previous power values to consider
                                %when running the smoothing algorithm
                                %(denoted N in report).
seconds_per_sample = 0.0025;     %Simulation time step.
sampel_per_second = 1/seconds_per_sample; %Samples per second.
watt_per_sample_allowed = power_slope_allowed/sampel_per_second; %Maximum
                                %allowed increase in watt between samples
                                %to ensure the maximum ramp rate.
watt_per_power_vector_length_allowed =  watt_per_sample_allowed *...
    (delta_power_vector_length - 1); %Maximum allowed increase in watt
                                %between the the present and the power
                                %value N iterations before.
summing_vector = linspace(1,(delta_power_vector_length - 1),...
    (delta_power_vector_length - 1)); %Vector of power differences between
                                %present and previous values if ramp rate
```

```
                                %is 1 W/sample (slope = 1).
sum_delta_power_vector = sum(summing_vector); % Sum of power differences
                                %between present and previous values if
                                %ramp rate is 1 W/sample (slope = 1).
p_trigger = sum_delta_power_vector * watt_per_sample_allowed; %Scaled
                                %value of the sum of power differences that
                                %gives the trigger value for the smoothing
                                %algorithm. If the sum of power differences
                                %is higher than this values, smoothing
                                %should be activated.
power_vector = zeros(1,delta_power_vector_length); %Initial power vector.
delta_power_vector = zeros(1,delta_power_vector_length); %Initial
counter_1 = 0;                  %Initial value of help variable in the
                                %smoothing algorithm.
counter_2 = 0;                  %Initial value of help variable in the
                                %smoothing algorithm.

smooth_on_indicator = zeros(1,10); %Vector allowing for detection of
                                %previous activations of smoothing.
counter_3 = 0;                  %Initial value of help variable in the
                                %smoothing algorithm.

%%END Create parameters for smoothing algorithm----------------------------

%%Function for the MPPT/smoothing block in the Simulink model--------------

function [voltage_ref] = mppt_v70_final(voltage_mppt,current_mppt) %Input
                                    %is voltage and current from the PV
                                    %panel, output is a new voltage
                                    %reference.
%Evaluate and set variables-----------------------------------------------

voltage_ref = voltage_mppt;         %Initial value for voltage reference is
                                    %set to the present voltage input.
mppt_step_size = evalin('base','mppt_step_size'); %Make predefined step
                                    %size is accesable.
voltage_mppt_prev = evalin('base','voltage_mppt_prev'); %Make previous
                                    %voltage accesable.
current_mppt_prev = evalin('base','current_mppt_prev'); %Make previous
                                    %current accesable.
delta_I = current_mppt - current_mppt_prev; %The difference between present
                                    %and previous current is calculated.
delta_V = voltage_mppt - voltage_mppt_prev; %The difference between present
                                    %and previous current is calculated.

%END evaluate and set variables-------------------------------------------

%Smoothing algorithm------------------------------------------------------

power_vector = evalin('base','power_vector');%Make power vector accessible.
p_trigger = evalin('base','p_trigger'); %Make the maximum sum of power
                                    %differences accessible.
delta_power_vector = evalin('base','delta_power_vector'); %Make power
                                    %difference vector accessible.
delta_power_vector_length = evalin('base','delta_power_vector_length');
                                    %Make the length of the power vector
                                    %accessible.
counter_1 = evalin('base','counter_1'); %Counter to hold the smoothing
                                    %algorithm during initial iterations.
counter_2 = evalin('base','counter_2'); %Counter to fill the power vector
```

```
                                    %and power difference vector correctly
counter_3 = evalin('base','counter_3'); %Counter used to track if smoothing
                                    %is activated last 10 iterations.
counter_3 = counter_3 + 1;          %Increasing counter.

if counter_3 == 11                  %Resetting counter if exceeding 10.
    counter_3 = 1;
end

assignin('base', 'counter_3', counter_3); %Save variable.
smooth_on_indicator = evalin('base','smooth_on_indicator'); %Make the
                                    %vector accessible that indicating if
                                    %smoothing has been active within 10
                                    %iterations.
if counter_1 < delta_power_vector_length + 1 %Increasing counter during the
    counter_1 = counter_1 + 1;      %initial iterations.
    assignin('base', 'counter_1', counter_1);
end

counter_2 = counter_2 + 1;          %Increasing counter.
power_vector(counter_2) = voltage_mppt * current_mppt; %Saving present
                                    %power value in a power vector.
assignin('base', 'power_vector', power_vector); %Saving power vector.

if counter_1 > delta_power_vector_length %Holding the smoothing
                                    %algorithm during initial iterations.
    for a = 1:delta_power_vector_length %Fill the power difference vector
                                    %with the power differences between the
                                    %present and previous power levels.
        delta_power_vector(a) = power_vector(counter_2) - power_vector(a);
                                    %When same element, the difference will
                                    %be zero - this is accounted for.
    end
    delta_power_vector_sum = sum(delta_power_vector); %Summing the power
                                    %differences.
    if delta_power_vector_sum >  p_trigger % Checking if smoothing should
                                    %be activated.
        smooth_on_indicator(counter_3) = 1; % Setting one element in the
                                    %smoothing indicator vector to 1, this
                                    %to indicate an activation of smoothing
        assignin('base', 'smooth_on_indicator', smooth_on_indicator); %Save
                                    %smoothing indication vector.
        if mppt_step_size > 0.01    %Reduce voltage reference step size by
                                    %0.002 V if previous step size is
                                    %larger than 0.01 V.
            mppt_step_size = mppt_step_size - 0.002;
            assignin('base', 'mppt_step_size', mppt_step_size);
        end

        voltage_ref = voltage_ref + mppt_step_size; %Increase voltage
                                    %reference to achieve power limitation.

        assignin('base', 'current_mppt_prev', current_mppt); %Save present
                                    %current value.
        assignin('base', 'voltage_mppt_prev', voltage_mppt); %Save present
                                    %voltage value.
        if counter_2 == delta_power_vector_length %Reset counter if length
                                    %of the power vector exceeds 60 (N).
            counter_2 = 0;
```

```
        end
        assignin('base', 'counter_2', counter_2); % Save counter value.

        return; %End the function and output new voltage reference.

    elseif mppt_step_size < 0.25    %Increase voltage step size if it was
                                    %previously lower than 0.25 V and if
                                    %smoothing has not been active within
                                    %the 10 last iterations.
        if sum(smooth_on_indicator) < 1
            mppt_step_size = mppt_step_size + 0.005;
            assignin('base', 'mppt_step_size', mppt_step_size);
        end

        smooth_on_indicator(counter_3) = 0; %Reset counter.
        assignin('base', 'smooth_on_indicator', smooth_on_indicator); %Save
                                    %counter value.

    else

        smooth_on_indicator(counter_3) = 0; %Reset counter.
        assignin('base', 'smooth_on_indicator', smooth_on_indicator); %Save
                                    %counter value.
    end
end

if counter_2 == delta_power_vector_length %Reset counter if length
                                    %of the power vector exceeds 60 (N).
    counter_2 = 0;
end

assignin('base', 'counter_2', counter_2); %Save counter value.

%END smoothing algorithm-----------------------------------------------------

%MPPT algorithm--------------------------------------------------------------

if delta_V == 0                     %Checking if the voltage-difference is
                                    %zero
    if delta_I == 0                 %Checking if the current-difference is
                                    %zero. If it is, then operation is at
                                    %MPP and no change in voltage reference
                                    %is made.
        %Do nothing
    elseif delta_I > 0

        voltage_ref = voltage_ref + mppt_step_size; %If current difference
                                    %is > 0 the new voltage reference is
                                    %increased with a predefined step size.
    else
        voltage_ref = voltage_ref - mppt_step_size; %If current-difference
                                    %is < 0 the new voltage reference is
                                    %decreased with a predefined step size.
    end
elseif delta_I/delta_V == -current_mppt/voltage_mppt %If the incremental
                                    %conductance = minus the instantaneous
                                    %conductance, then operation is at MPP
                                    %and no change in voltage reference is
                                    %made.
```

```
    %Do nothing
elseif delta_I/delta_V > -current_mppt/voltage_mppt
    voltage_ref = voltage_ref + mppt_step_size; %If the incremental
                                    %conductance > minus the instantaneous
                                    %conductance, the new voltage reference
                                    %is increased with a predefined step
                                    %size.
else

    voltage_ref = voltage_ref - mppt_step_size; %If the incremental
                                    %conductance > minus the instantaneous
                                    %conductance, the new voltage reference
                                    %is decreased with a predefined step
                                    %size.
end
assignin('base', 'current_mppt_prev', current_mppt); %The present current
                                    %value is saved for comparison in next
                                    %iteration.
assignin('base', 'voltage_mppt_prev', voltage_mppt); %The present voltage
                                    %value is saved for comparison in next
                                    %iteration.

return;                             %The function outputs a (new) voltage
                                    %reference.

%END MPPT algoritm-------------------------------------------------------

%%END Function for the MPPT/smoothing block in the Simulink model----------
```